aerospace

MDPI

Review

Test Activities on Hybrid Rocket Engines: Combustion Analyses and Green Storable Oxidizers—A Short Review

Christian Paravan *, Anwer Hashish and Valerio Santolini

Space Propulsion Laboratory (SPLab), Department of Aerospace Science and Technology, Politecnico di Milano, 20156 Milan, Italy

* Correspondence: christian.paravan@polimi.it; Tel.: +39-02-2399-8058

Abstract: Hybrid rocket engines (HREs) offer a low-cost, reliable, and environmentally friendly solution for both launch and in-space applications. Hybrid propellants have been identified as green thanks to their use of non-toxic, non-carcinogenic oxidizers. Of particular relevance are storable oxidizers, namely high-concentration (≥90 wt.%) hydrogen peroxide (HP, H_2O_2) and nitrous oxide (N_2O). This work provides a survey of experimental activities based on H_2O_2 and N_2O for hybrid rocket propulsion applications. Open literature data are completed with original thermochemical calculations to support the discussion.

Keywords: green propellants; storable oxidizers; hybrid rocket engine; hydrogen peroxide; nitrous oxide; combustion; environmental impact; greenhouse effect; launch system; in-space propulsion

Citation: Paravan, C.; Hashish, A.; Santolini, V. Test Activities on Hybrid Rocket Engines: Combustion Analyses and Green Storable Oxidizers—A Short Review. *Aerospace* **2023**, *10*, 572. https://doi.org/10.3390/aerospace10070572

Academic Editor: Stephen Whitmore

Received: 19 May 2023
Revised: 10 June 2023
Accepted: 15 June 2023
Published: 21 June 2023

1. Introduction

In the field of thermochemical propulsion, a propellant is defined as *green* if it has characteristics of low (if any) toxicity and easy and safe transportation and handling. In addition to this, a green propellant should provide the lowest possible emission levels during its lifecycle, from production and storage to the interaction of its exhaust combustion products with the external environment. Interest in green propellants has been furthered by ever-deeper environmental responsibility and requirements for a reduction in humanity's impact on environment. The development of green propellants is fostering advances in thermochemical propulsion. In this latter field, the major causes of environmental impact can currently be identified as: (i) ammonium perchlorate (AP) in solid propellant propulsion systems; and (ii) hydrazine/hydrazine-derived liquid propellants. The former raises environmental concerns due to the presence of HCl in its exhaust, as well as the possible influence of condensed combustion products (CCPs) on ozone depletion [1–4]. Propellants based on hydrazine and nitrogen tetra-oxide require complex (and expensive) handling procedures, with criticalities in cases of accidental release or emergency dumping [5–7].

Hybrid rocket engines (HREs) are typically presented as having a low environmental impact and being safe propulsion systems [8]. HREs usually burn solid hydrocarbon fuel with a liquid oxidizer (gaseous oxidizers are considered in lab- and small-scale applications). Therefore, the main exhaust products of HREs are CO, CO_2, and H_2O. The environmental impact reduction of HREs has been evaluated by contrasting them with the toxic and polluting emissions of AP-based solid rocket motors and the hazardous handling of hydrazine-based propellants. The high safety of HREs is due to their use of inert fuel grains during manufacture and transportation, and to their tolerance to grain cracks thanks to their peculiar combustion behavior. The combustion of conventional (polymeric) fuels as hydroxyl-terminated polybutadiene (HTPB) shows slow regression rates, therefore limiting the thrust produced by HREs with simple grain geometries (i.e., single, central port cylindrical grains). This is a critical point for the implementation of HREs in launch systems. Liquefying fuels offer a faster solid-fuel regression rate (r_f) than polymeric

formulations [9,10]. However, these fuels suffer from unsuitable thermomechanical properties [11]. Currently, HREs are typically conceived for small and medium launch vehicles, space tourism, and in-space propulsion applications [12,13]. Liquid oxygen (LOX) is the most performing oxidizer in terms of theoretical specific impulse and r_f performance [14]. However, because it requires low temperatures (90 K), LOX complicates the overall HRE design while limiting system storability and requiring relatively complex fluidic line design (injection/atomization and grain ignition). The use of storable oxidizers reduces some of the critical points related to the use of cryogenic liquids for both launch and in-space applications. Oxidizers such as N_2O and H_2O_2 (at different concentrations) offer interesting features such as exothermic decomposition (with the possibility of a simplified design of the engine ignition system) and relatively high oxygen content. This work provides a review of the open literature dealing with the analysis and testing of storable propellants in HRE development, with a focus on liquefying fuels. Analyses and studies are critically discussed to provide readers with a green perspective on HREs. Highlighting the role of liquefying fuels, and, in particular, of paraffin-based fuels is a choice based on the overall relevance of these fuels for both launch and in-space applications, and on their theoretical flame temperature/specific impulse performance, which shows no significant difference to conventional fuels such as HTPB [14]. In the discussion, fundamental aspects of hybrid rocket combustion are introduced first. Then, after a short presentation of the most relevant physical properties of storable oxidizers and a short analysis of thermochemical performance of propellants of interest, combustion tests of N_2O and H_2O_2 with solid fuel are reviewed.

Finally, conclusions are presented, together with some recommendations for future developments.

2. Hybrid Rocket Combustion

The Figure 1 shows the conventional configuration of an hybrid rocket engine. Pioneering efforts in the study of solid-fuel combustion in HREs began in the first half of the 20th century. Altman and Holzman [14] offer a comprehensive review, covering hybrid propulsion milestones from its inception to the most recent achievements. Interestingly, earlier efforts in hybrid propulsion used N_2O (Andrussow, Lutz, and Noggerath at I.G. Farben in 1937), and H_2O_2 (Moore and Berman at General Electric from the late 1940s to the mid-1950s) [14].

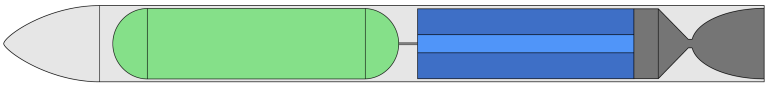

Figure 1. Simplified scheme of HRE with conventional configuration: the (liquid/gaseous) oxidizer tank is shown in green, while the solid-fuel grain (with a single central port perforation) is in blue.

The following subsections provide: (i) a discussion of the fundamentals of hybrid rocket combustion, starting from early studies on conventional fuels and covering the most recent efforts; (ii) combustion enhancement techniques; (iii) an introduction to some peculiarities of HREs, such as soot production and, in particular, the oxidizer-to-fuel ratio (O/F) shift effects; and (iv) a brief review of environmental studies in the rocket industry. Treatment in this section is mainly conducted considering gaseous oxygen as an oxidizer, as per lab- and small-scale activities typical of early fundamental studies. However, when N_2O and H_2O_2 combustion is encountered in references dealing with the topics (i)–(iv), a discussion of the relevant publications is performed in Section 3.

2.1. Fundamentals

The combustion of conventional fuels occurs in a boundary layer created by an oxidizer stream over a condensed phase surface. Vaporized fuel diffuses from a regressing surface to an atomized/gaseous oxidizer flow. A diffusion flame transfers heat into a condensed phase by convection and radiation. Mass blowing from the grain surface hinders the convective

heat transfer (i.e., blockage effect). Radiation heat transfer from gaseous combustion products exerts a limited influence on the combustion process of non-metalized fuels. For conventional fuels, the r_f is relatively slow. Marquardt and Majdalani [15] provide a review of turbulent boundary layer combustion models. In the field of HRE combustion modeling and analysis, the early efforts of Marxman and co-workers [16–18] still play a central role. A series of efforts toward detailed analyses was made by the Pennsylvania State University research group and is well presented by the authors in [8]. In HRE combustion, the regression rate is related to the total (i.e., propellant) mass flux (G) by a power-law relationship, as follows:

$$r_f = a_r G^{n_r} \tag{1}$$

with $n_r = 0.8$ for a purely turbulent convective heat-transfer regime. Equation (1) is typically used in a slightly different form, considering the oxidizer mass flux (G_{ox}) as the controlling parameter. In actual testing conditions, the n_r exponent shows differences regarding the purely convective regime, with values in the range 0.6–0.8 [8]. This is partially due to the influence of radiation heat transfer that is possibly caused by: (i) fuel-rich O/F, implying the presence of highly emitting soot particles; and (ii) relatively low total (or oxidizer) mass fluxes yielding reduced convective heat transfer. Discussion on the impact of radiation heat transfer in lab-scale HREs with pure hydrocarbon fuels has been led by Strand et al. [19], Chiaverini et al. [20], and Estey et al. [21]. It is worth noting that with reduced G, the impact of radiation can be significant, yielding an r_f dependence on combustion-chamber pressure p_c (indeed, on $p_c \cdot D$, with D = port diameter). Combustion pressure effects on r_f are also possible for high G values when chemical kinetics starts playing a significant role. Finally, a diffusion flame implies relatively low combustion efficiencies due to difficult oxidizer–fuel mixing. This possibly affects the emissions of HREs, unless specific correcting actions/designs are pursued. Advanced studies for HRE development tackle issues related to slow r_f and combustion efficiency.

2.2. Studies on Combustion Performance Enhancement

Combustion performances of HREs include: (i) the r_f; and (ii) the combustion efficiency. Although high-enough combustion efficiencies are pursued in both launch systems and in-space applications, the research for faster r_f is typical of the access to space systems. The following treatment focuses on r_f enhancement first. Then, efforts for higher combustion efficiencies are presented.

Several techniques have been proposed for the r_f enhancement of conventional fuels. These include (in non-chronological order of development): (i) the use of liquefying fuel formulations; (ii) solid-fuel loading with high-energy-density fuels as metal and hybrid powders; (iii) the implementation of exotic oxidizer-injection methods; (iv) heat-transfer increase by the alteration of grain surface roughness and port shape. Recent reviews of the topic have been carried out in [11,22–27].

The use of AP (or other oxidizers) as an additive for ballistic performance enhancement has been proposed too [25,26]; however, this solution is not considered in detail in this review due to its implications for the effects of Cl on the exhaust, or the possible detriment of intrinsic HRE safety. Focusing on r_f and combustion efficiency enhancement, the following discussion does not consider multiport configurations, where high thrust levels are pursued by increasing the regressing surface area. The reason behind this choice is that the method has been widely investigated in the past, demonstrating volumetric efficiency criticalities, despite some relevant results in terms of generated thrust [28].

Liquefying formulations offer enhanced r_f thanks to the entrainment mass transfer of the melted fuel. In these kinds of fuels, grain melts under the enthalpy transfer from the flame. Depending on the pressure regime, the surface layer (liquid at subcritical conditions, fluid in the supercritical regime) is unstable under the shear action of the propellant stream: the behavior is connected to the surface-layer low viscosity (and, in subcritical conditions, surface tension) [9,10,29,30]. As a result of the low stability, the melted fuel is sprayed into the propellant stream. Therefore, this mechanism provides an additional contribution to the

surface vaporization regression. Originally reported in [31], the entrainment mechanism was first justified and detailed in [9,10].

A detailed analysis on entrainment in hybrid rocket engines is reported by the authors in [29,30,32,33]. Entrainment provides mass transfer from the regressing grain without contributing to convective heat-transfer blockage. Therefore, r_f of up to four times that of conventional formulations can be achieved [9,30,34–39]. Paraffin waxes are a class of liquefying fuels of particular interest thanks to their availability and ease of handling. The poor mechanical properties of pure paraffin require improvements before they are suitable for operating conditions during launch and in-space operations. Blending wax with thermoplastic polymers is the strategy commonly pursued for this purpose [11,25,35–38,40–43]. Such a reinforcement, as well as the use of HTPB (or another thermosetting matrix) [44,45], produces significant effects on the mechanical response of fuel only for relatively high blending-polymer mass fractions. This high-polymer load implies a reduction in entrainment mass transfer due to increased melt fuel viscosity. Evaluation of the r_f dependence on the melt fuel viscosity is reported in [38,40–43].

The achieved results show $r_f \propto \mu^n$, with n in the range -0.2 to -0.3. Recently, an innovative method for fuel-grain reinforcement has been proposed [46]. The method exploits 3D printing to generate cellular structures that are embedded in the paraffin–fuel matrix. The structure provides mechanical reinforcement, therefore preventing (or limiting) paraffin blending [46,47]. Results for a gyroid structure printed in acrylonitrile butadiene styrene (ABS) with a 15% infill and embedded in a microcrystalline wax matrix show a yield strain increase of 213%, with the grain mechanical behavior turning from brittle to ductile. For the same matrix, the embedded ABS structure promotes r_f increases in the range of 60 to 90% (depending on reinforcement infill).

In HRE applications, solid-fuel loading with energetic additives has r_f (and the mass burning rate) enhancement as the main driver [11,22,23,48,49]. In contrast to solid rocket motors, metal and metal hydride powders show no marked increase in the theoretical specific impulse of HREs. Such a result is well discussed in [50,51], where experimental data considers oxygen as the oxidizer.

In particular, focusing on Al powders, the active metal content of the energetic filler has nearly no impact on the theoretical specific impulse of HRE [51]. When considering metal fuels for performance enhancement, a correct evaluation of the possible drawbacks should be pursued (i.e., two phase-flow losses due to CCPs). These considerations are complicated by the lack of detailed analyses in the open literature: no experimental investigations on the particle size and size distribution of condensed products from the combustion of HREs are available (though some considerations can be inferred from the experience on solid rocket motors [52,53]). However, in HREs, in contrast to solid rocket motors, particles are added with small mass fractions, with a limited impact on the (expected) condensed species' mass fractions [50,51]. In conventional formulations, the accumulation of partially oxidized metal at the regressing surface has been identified as a limiting factor for regression rate enhancement [23,48]. Recent studies on the combustion behavior of metalized fuel formulations show limited performance enhancement for conventional formulations, typically <60%, featuring oxidizer mass flux dependence [54–56]. Experimental analyses considering paraffin-based fuels (in particular, paraffin–polyethylene blends) are reported in [57].

In this latter work, the use of micron-sized Al (nominal particle size in the range 10 to 20 μm) in paraffin blends provided faster r_f than for its non-metalized counterpart. However, under the investigated conditions (GOX, G_{ox} = 100 kg/m^{2}s), the percentage r_f enhancement achieved by a 25 wt.% metal load of a 10 wt.% polyethylene blend is within the previously reported range, with pure paraffin outperforming compared to the metalized blends.

Swirl and vortex flow injection enables r_f enhancement [58–60], increases combustion efficiency [36,61–63] and reduces the pressure oscillations/low-frequency instabilities observed in small-scale engines [8,58,59]. The main limitations of this approach are related to

swirl decay along the fuel grain due to viscous dumping [8,58,61,64]. For in-space applications, this issue can be addressed with non-conventional engine configurations, such as the exotic vortex flow pancake (VFP) [36,63,65]. The VFP features a length-to-diameter ratio <1, thus limiting vortex intensity losses along the combustion chamber while offering high combustion efficiencies (∼99% in terms of characteristic velocity).

Focusing on conventional engine geometry, according to the data reported in [59,60], r_f increases of up to 270% are achieved for a swirl geometrical number of 19.4 and classical fuel.

A scaling analysis for swirl injection is presented by Paccagnella et al. [61]. Swirl injection effects on the ballistic response of solid fuels are investigated in [66–68]. Although general comments presented for conventional fuels are confirmed by these analyses, in [67] the authors highlight how the sensitivity of wax fuel to swirl injection results is stronger than that of conventional compositions.

An interesting combination of swirl and standard injection is proposed in the A-SOFT (altering-intensity swirling-flow-type) HRE [69–71]. This peculiar engine is under development, and proposes a tailoring of the injection conditions to control thrust at an optimal oxidizer-to-fuel-mass ratio while achieving relatively fast regression rates with a fixed motor configuration.

Enhanced fuel–oxidizer mixing can be promoted by special grain configurations and devices. Effects on the combustion efficiency of diaphragms are discussed by Grosse [72]. In this work, N_2O is considered to be an oxidizer: these results are discussed in detail in Section 3. Exotic grain configurations with a single central port with helical geometry [27,73] and engines with peculiar grain segmentation [74,75] have been proposed for enhanced combustion performance. For the former, a series of experimental data on ABS combustion is available, while, for the latter, the open literature reports no regression rate or combustion efficiency data. In [27], helical port geometry favors r_f enhancement thanks to: (i) increased skin friction; and (ii) the reduction of wall-blowing using centrifugal effects induced by the helix pitch. Regression rates of up to four times those of conventional port configurations were achieved using this method for 3D-printed ABS grains. As clarified by the engineering model developed by the authors in [73], 75% of the overall regression rate enhancement is due to the increased skin friction, with 25% of the performance gain being due to the reduced wall-blowing. Unfortunately, during combustion, grain consumption gradually erases the helical configuration of the port, reducing the r_f enhancement [27].

2.3. The O/F Shift, Condensed Combustion Products, and Soot

In typical HRE configurations, the overall $O/F(t)$ changes over time. This effect is due to $r_f(G_{ox})$ and the regressing surface evolution during the combustion. For a cylindrical grain with a single central port perforation, $O/F(t)$ increases in time for $n_r > 0.5$ (with neutral and regressive behaviors being related to $n_r = 0.5$ and $n_r < 0.5$, respectively). As a result of the O/F shift, the specific impulse of the system changes during engine firing. The phenomenon is well known, though few studies have focused on its effects on engine performance. A discussion on the influence of O/F shift on performance is reported in [76]. This analysis includes data from different single- and multiport configurations [76]. Results show how the cylindrical grain with single-port perforation exhibits no significant performance detriment during burning due to the O/F shift in terms of combustion efficiency. However, the phenomenon must be taken into account during engine design, since suitable time-averaged O/F should characterize the firing.

The open literature lacks detailed studies on the impact of CCPs on the actual gravimetric specific impulse values. However, solid-fuel formulations typically show limited additive mass fractions (in particular, in the case of entrainment-producing compositions, where the energetic filler typically increases the melt fuel viscosity [77]). Therefore, a limited impact of CCPs on the expansion process of loaded HRE propellants is expected. Similarly, the use of a relatively small additive mass fraction suggests limited environmental effects, such as ozone depletion mechanisms fostered by metal oxides.

Soot formation is a critical aspect of HRE combustion. However, the open literature lacks detailed studies offering an assessment/estimation of its impact on actual systems. Considering the O/F shift, and the peculiar combustion mechanism of HREs, the fuel may burn in fuel-rich conditions favoring soot formation. Detailed analyses on this point depend on the specific system/operating conditions under scrutiny, and cannot be generalized. Although soot formation is a kinetically driven phenomenon, thermochemical equilibrium also foresees the possible insurgence of condensed carbon from fuel combustion when the carbon-to-oxygen ratio exceeds unity, as reported by De Luca et al. [12]. A recent analysis of the impact of oxygen concentration effects on soot production is discussed by Aphale et al. [78]. In this study, the analysis focuses on polymethyl methacrylate burning under different oxygen concentrations spanning from 17% to 100%. The final aim of the study reported in [78] is an evaluation of the impact of radiation heat transfer on r_f. Under the investigated conditions, soot production is observed to increase with increasing oxygen mass fraction up to 45% O_2, with a subsequent decrease. Under these circumstances, the radiation heat transfer monotonically increases, due to flame temperature enhancement, with increasing oxidizer content. Few studies have tackled the problem of exhaust plume analysis for HREs [79]. In addition to this, the open literature offers scarce investigations (if any) of the after-burning effects of HRE plumes.

2.4. Environmental Impact

Air pollution is defined as the change in the natural composition of atmosphere. In this sense, combustion processes have a strong impact. In the troposphere, thermochemical rocket emissions are negligible compared with aviation and the other sources [80–82]. On the other hand, they are the only cause of pollution at higher altitudes. Thus thermochemical rocket propulsion is fully responsible for the human impact on the stratosphere. In the upper atmosphere, rocket combustion may affect the stratosphere equilibrium mainly in two ways: (i) the greenhouse effect; and (ii) ozone-layer breakdown.

The former is caused by the response of molecules to short-wave radiation (by the Sun) and long-wave radiation (infrared, by the Earth). Greenhouse gases are transparent to short waves but tend to absorb longer waves. Atmospheric gases responsible for this effect are water vapor (H_2O), carbon dioxide (CO_2), and ozone (O_3). Normally, if annual global radiated energy is equal to the level of solar energy absorbed, the Earth's temperature is in global equilibrium. The artificial introduction of more CO_2 and H_2O or of nitrogen oxides (NOx), CO, CH_4, UHC, and soot might alter this equilibrium [83].

Ozone can be found all over the atmosphere, but it has its maximum concentration between an altitude of 25 and 35 km [83]. There, the thick O_3 layer acts as a solar ultraviolet (UV) radiation filter. Ozone is an unstable gas formed by the chemical reaction of O_2 and O chemical in which, under nominal atmospheric conditions, the direct and reverse reactions are in equilibrium. The introduction of chlorine and bromide compounds, as well as N_2O and NOx, which act as catalysts in ozone depletion, alter this equilibrium, causing the so-called "ozone hole" phenomenon.

The effects of chemical rockets on the environment have already been investigated during the Space Shuttle program [84–86] and were later reviewed by the authors in [4]; many issues have been addressed. The Space Shuttle's major chemical products at the nozzle exit were: (i) HCl, Al_2O_3, H_2, H_2O, CO, and CO_2 for the solid rocket boosters (typical solid fuel); and (ii) H_2 and H_2O for the main engines working with LOX and liquid hydrogen (LH_2). A model to analyze the effects of exhaust gases reacting with the atmosphere is reported in [87]. Results highlighted the danger of the use of Cl in rockets for ozone depletion. However, LOX/LH_2 green products also react when mixed at high temperatures with the surrounding atmosphere. This reaction leads to the production of nitric oxide, responsible for O_3 dissociation. However, this amount of NO is negligible compared to the direct introduction of chlorine [87]. Results suggest a deeper investigation into atmosphere interaction with exhaust plume gases when operating hybrid rocket

engines (usually operating at a high O/F ratio) employing N_2O or H_2O_2 as oxidizers. Studies about this topic are not currently present in the literature.

Due to the relatively recent diffusion of hybrid engines, few studies are available about their environmental impact. Discussion from [88] yields to consider HRE direct emissions as less impacting than other rocket engines when focusing on the greenhouse effect.

Whitmore et al. [79] carried out a comparison between hydrazine (N_2H_4) and the ABS-gaseous oxygen (GOX) propulsion system's plume species. For the hybrid engine, dominant combustion products at the nozzle exit are CO, CO_2 and H_2O when operating at an equivalence ratio range of $1.35 < \Phi < 2.25$, with negligible production of C(gr). CO is characterized by little contamination risk, and CO_2 and H_2O mass concentrations vary between 10 and 35%. The contamination potential is relevant, but the hybrid engine results cleaner than hydrazine, which is characterized by condensable species varying from 40 to 50% mass concentrations.

A study on the emissions from the mission profile of a LOX/paraffin three-stage hybrid launcher is reported in [82]. The NASA-CEA code is used for the analysis. Considering the methods implemented in [82] improvements in the emission functions developed in [88] were achieved. Combustion products at the nozzle exit are obtained as a function of the trajectory without requiring the hypothesis of pollution distribution along atmospheric altitude [82]. In [82], Al impact is not accounted for since it is not present in the fuel, greatly lowering the environmental impact [88]. Carbon soot is neglected because it is obtained only for O/F< 1.2 (far from operating conditions). Major mass fractions are obtained for CO, CO_2, and H_2O. The instantaneous radiative force (iRF) for the latter two is computed using models formulated by the authors in [88]. The carbon footprint (CFP) is computed from the global warming potentials (GWP). CO and CO_2 are the only two major gases with a GWP$\neq 0$, with $GWP_{CO_2} = 1$ and $GWP_{CO} = 3$ [81]. Results show a total $CFP = 6636$ kg, an $iRF_{CO_2} = 4.9 \cdot 10^{-12}$ mW/m^2, and an $iRF_{H_2O} = 1.0 \cdot 10^{-8}$ mW/m^2. A -25% CFP and -10% iRF can be achieved by a -10% payload mass reduction [82].

Further studies should move in the direction of expanding the plume-atmosphere interaction developed in [87] to hybrid rocket engines, to understand their effect on ozone depletion, especially when using N_2O as an oxidizer. Additionally, if considering the results of in [82] and the results reported in the Section 3, a deeper investigation of the impact on radiation forces when using H_2O_2 as an oxidizer should be conducted.

3. Green Storable Oxidizers

When pursuing high performance in terms of r_f and specific impulse, LOX has always been an attractive opportunity for HRE designs. The most powerful HRE to date (rated 1.1 *MN* thrust) was designed and built by the American Rocket Company (AMROC) using the aforementioned oxidizer and HTPB as fuel [28]. Recently, HyImpulse, a German start-up developing sounding rockets and planning the development of a three-stage launch vehicle for the orbit insertion of payloads of up to 500 kg, is considering LOX for its applications. A 75 kN demonstrator, HyPLOX75, was successfully fired in a static test in September 2020 [89]. As a side advantage in the small- to large-scale applications, LOX burning behavior can be related to a variety of lab-scale datasets employing gaseous oxygen as the oxidizer. However, the use of LOX requires complex handling and implementations, due to its cryogenic nature. Trends in the propulsion market regarding the possible exploitation of HREs in small- to medium-size launchers promote interest in storable oxidizers such as hydrogen peroxide [90,91] and nitrous oxide [90]. Therefore, the open literature research and relevant operating realizations identify N_2O and H_2O_2 as the current candidates for affordable hybrid propulsion systems [92–94]. Historically, other storable oxidizers have been investigated for HRE applications, such as nitrogen tetroxide (N_2O_4), nitric acid (HNO_3, NA), and red-fuming nitric acid (RFNA). However, presently, these reactants are not considered in the perspective of commercial applications due to them raising significant environmental concerns [14].

Table 1 presents an overview of the most relevant properties of cryogenic and storable oxidizers. For hydrogen peroxide, two different concentrations are considered: 90 wt.% and

98 wt.%. As reported by Whitmore [95], the use of H_2O_2 with a concentration >90 wt.% makes the definition of a green propellant only slightly applicable (see also [96]). However, high concentrations of hydrogen peroxide are typically accepted as green reactants.

Thermochemical computations are hereby reported as connections between Sections 2 and 3. The analysis takes into account paraffin wax, widely considered in lab- and small-scale testing, burning with storable oxidizers. The presented data include the reference case of a cryogenic oxidizer.

Figure 2 provides a comparison of specific impulse performances between cryogenic and storable oxidizers. The reported data shows the reduced gravimetric specific impulse performance of H_2O_2 and N_2O compared to LOX. Data from Table 1 show the attractive density of H_2O_2 over N_2O and LOX. This feature, together with the higher gravimetric specific impulse, suggests a better suitability of this oxidizer over nitrous oxide when the final application requires high volumetric efficiency. However, both storable oxidizers provide the possibility of HREs with equivalent or superior performance compared to AP-based solid propellants, whose theoretical specific impulse in the same conditions of the data reported in Figure 2 is in the range of 1952 m/s to 3092 m/s for a typical commercial formulation with 68 wt.% AP, 18 wt.% micron-sized Al, and 14 wt.% HTPB. Focusing on the possible use of HREs in in-space applications, the peak values of the gravimetric specific impulse are comparable with those of hydrazine–nitrogen tetroxide storable propellants (in the range of 1556 m/s to 2296 m/s under similar operating conditions). In contrast to LOX-based systems, HREs based on N_2O and H_2O_2 feature relatively small variations of the gravimetric specific impulse over a relatively wide range of O/F (see Figure 2). However, for these systems, as well as for the cryogenic counterpart, it is possible to observe a specific impulse performance change when passing from fuel-rich to fuel-lean mixture ratios. Figure 3 provides an evaluation of the impact of this O/F shift on the emissions (as evaluated from a thermochemical equilibrium code). As discussed in Section 3, H_2O_2 and N_2O gravimetric specific impulse performances are not significantly affected by the addition of energetic additives. This is testified by the data reported in Figure 4, where Al is taken as the reference material, and in Table 2, where different additives are contrasted for a 10 wt.% load. The faint influence on the maximum specific impulse (with a corresponding small shift of the O/F at which the maximum performance is achieved) is accompanied by the presence of a small fraction of CCPs (typically <5 wt.%). Such a result suggests that solid-fuel loading with energetic additives should be considered as a strategy for regression rate tailoring, together with the possible implementation of non-conventional oxidizer-injection methods.

Table 1. Physical properties of storable oxidizers [71,97,98].

Property	HP 90 wt.%	HP 98 wt.%	N_2O	LOX
Active O_2 content [%]	42	46	36	100
Boiling point @ 1 atm [K]	414	422	185	90
Freezing point @ 1 atm [K]	261	270	182	54
Density @ [a] 293 K, 1 atm [g/cm^3]	1.395	1.431	0.786 [b]	1.141 [c]
Vapor pressure @ [a] 293 K [Pa]	200	133	5.0×10^6	9.9×10^4 [c]
Molar mass [g/mol]	32.4	33.7	44	32
Decomposition Temperature @ 2.0 MPa [K]	1029	1225	1907	N.A.

[a] Except where marked differently. [b] Liquid, @ $5.0 \cdot 10^6$ Pa (vapor pressure). [c] Liquid, @ 90 K (boiling temperature).

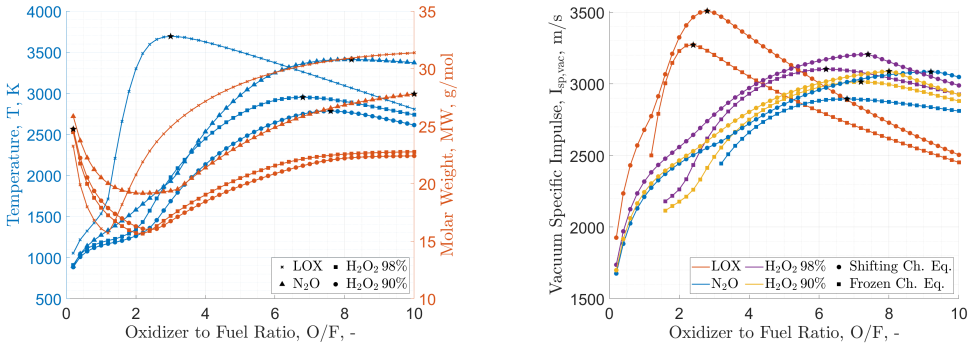

Figure 2. Cryogenic and storable oxidizers, theoretical performance by NASA-CEA code: adiabatic flame temperature and molar mass in the combustion chamber (left), vacuum specific impulse at exhaust (right). Paraffin-wax fuel ($C_{50}H_{102}$, heat of formation −1438.2 kJ/mol [72]). Calculations are performed for: (i) combustion-chamber pressure, $p_c = 7.0$ MPa, (ii) shifting chemical equilibrium and frozen chemical equilibrium (freezing @ throat), (iii) supersonic exhaust-to-throat-area ratio of 40. Maxima are highlighted by stars.

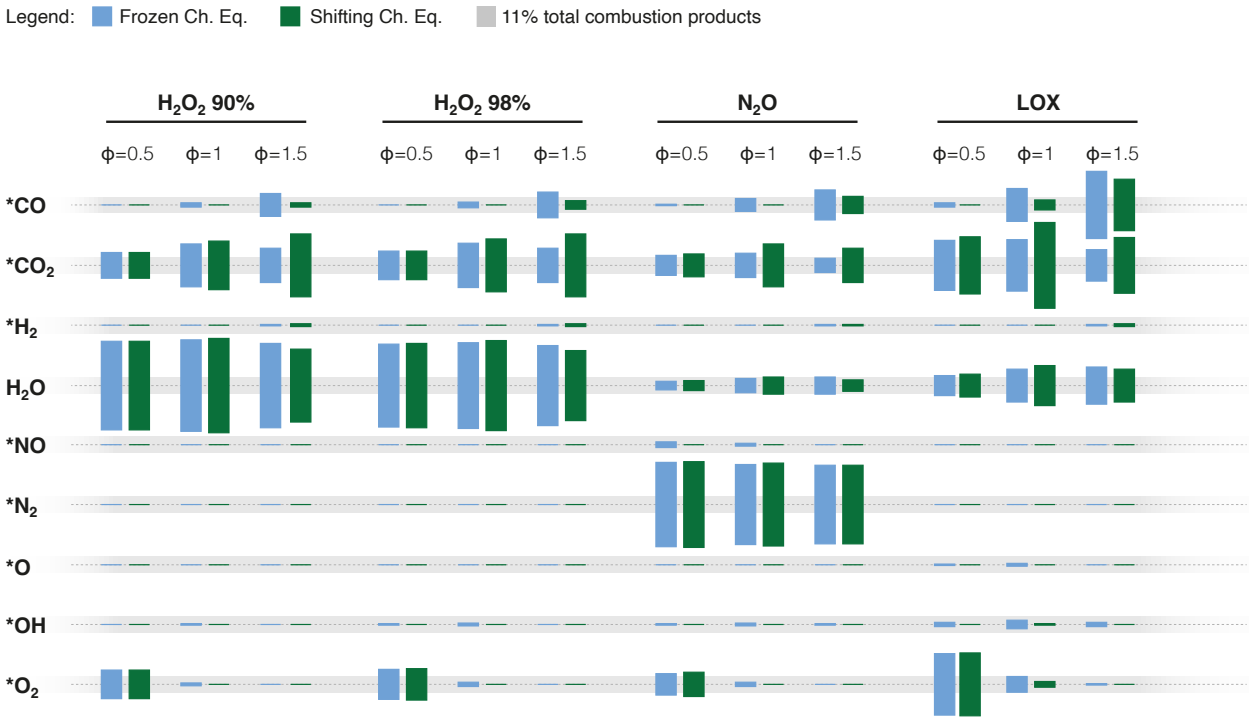

Figure 3. Exhaust composition from NASA-CEA for paraffin ($C_{50}H_{102}$, heat of formation −1438.2 kJ/mol [72]) burning with different oxidizers at equivalence ratios (Φ) in the range 0.5 to 1.5. Calculations are performed for: (i) combustion-chamber pressure, $p_c = 7.0$ MPa; (ii) shifting chemical equilibrium and frozen chemical equilibrium (freezing @ throat); and (iii) supersonic exhaust-to-throat-area ratio of 40. * NASA-CEA thermodynamic properties fitted to 20,000 K.

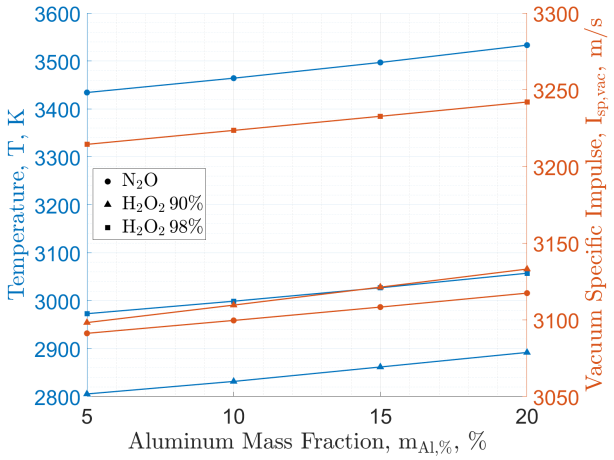

Figure 4. Paraffin fuel ($C_{50}H_{102}$, heat of formation −1438.2 kJ/mol [72]) burning with storable oxidizers: theoretical performance by NASA-CEA. Maximum adiabatic flame temperature and vacuum specific impulse at exhaust for increasing energetic additive mass fraction, with Al as a case study. Calculations are performed for: (i) combustion-chamber pressure, $p_c = 7.0$ MPa; (ii) shifting chemical equilibrium; and (iii) supersonic exhaust-to-throat area ratio of 40.

Table 2. Maximum vacuum specific impulse of paraffin fuel ($C_{50}H_{102}$, heat of formation −1438.2 kJ/mol [72]) loaded with 10 wt.% of different energetic additives. Corresponding oxidizer-to-fuel ratio and condensed combustion product mass fraction are reported. Calculations are performed for: (i) combustion-chamber pressure, $p_c = 7.0$ MPa; (ii) shifting chemical equilibrium; and (iii) supersonic exhaust-to-throat area ratio of 40.

Additive	**Oxidizer**								
	N_2O			**HP (90 wt.%)**			**HP (98 wt.%)**		
	$I_{sp,vac}$ m/s	**O/F -**	**CCPs wt.%**	**$I_{sp,vac}$ m/s**	**O/F -**	**CCPs wt.%**	**$I_{sp,vac}$ m/s**	**O/F -**	**CCPs wt.%**
-	3083	9.2	0	3087	8.0	0	3206	7.3	0
Al	3100	8.3	2.0	3110	7.4	2.2	3224	6.7	2.3
Mg	3091	8.3	2.9	3102	7.4	1.5	3215	6.7	1.1
AlH_3	3106	8.5	1.7	3116	7.6	1.9	3231	6.9	2.0
MgH_2	3091	8.5	1.5	3101	7.5	1.3	3215	6.8	0.9
$LiAlH_4$	3099	8.5	1.4	3111	7.6	1.5	3225	6.9	1.6

3.1. Nitrous Oxide

At ambient temperature, N_2O is liquid when stored at vapor pressure (see Table 1). In the following discussion, this is the default considered condition. Nitrous oxide features a high vapor pressure, with two main operating drawbacks: (i) a relatively low density; and (ii) a strong greenhouse impact (two orders of magnitude stronger than that of CO_2 [99]). The density of this liquid oxidizer is 30% lower than that of LOX (see Table 1). At the system level, the low volumetric efficiency of N_2O is partially mitigated when exploiting its high vapor pressure for self-pressurization.

Nitrous oxide exothermic decomposition into N_2 (∼66 wt.%) and O_2 (∼34 wt%) yields flame temperatures in the region of ∼1900 *K* (see Table 1). Thermal decomposition of the oxidizer occurs at temperatures of around 793 *K*, while a list of the possible catalysts for N_2O decomposition is given in [100–103]. Further considerations on N_2O physical properties are included and referenced in [104].

Nitrous oxide is one of the most commonly used oxidizers in HREs at the lab- and small scale (in particular, when dealing with sounding rockets). Moreover, it is the oxi-

dizer selected for one of the most relevant HRE realizations to date, namely the SpaceShipOne suborbital vehicle [14]. N_2O is widely used in relatively small systems since the cost-effectiveness trade-off, along with its high safety compared with other oxidizers, is favorable [105]. From the propulsion system design viewpoint, N_2O high vapor pressure (Table 1) allows the self-pressurization of the oxidizer. Therefore, N_2O offers the possibility to eliminate the additional weight, complexity, and cost of the pressurization system. The peculiarities of nitrous oxide decomposition are reviewed in [106].

Given the wide use of nitrous oxide in experiments and small-scale firings, a large $r_f(G_{ox})$ dataset exists. Table 3 provides an overview of the relevant results from the literature, considering the power-law fitting of the regression rate of Equation (1).

A wide series of lab-scale testing and hybrid sounding rockets were designed and implemented by Stanford University-related research groups [107–116]. The typical fuels considered in these efforts were paraffin wax and paraffin-based formulations.

In 2004, Van Pelt et al. [107] used paraffin with a N_2O oxidizer to launch a four-inch sounding rocket to nearly 1830 m. Then, in 2005, McCormick et al. [110] used paraffin loaded with 40 wt.% Al burning in N_2O to launch a 3 in (7.5 cm) sounding rocket to nearly 3050 m (10,000 ft).

Later, between 2006 and 2007, Lohner et al. [108] and Doran et al. [109] provided r_f data for N_2O in combination with conventional fuels (HTPB, PMMA, HDPE) and exotic formulations (SP1A—a paraffin wax, and Sorbitol—a sugar alcohol with chemical formula $C_6H_{14}O_6$). These lab-scale firings included the testing of metalized fuel formulations including micron-sized Al (nominal size 2 µm). Different Al loads (5 to 20 wt.%) were mixed with the fuels to observe the effects on the r_f. Experimental data from these two studies are not reported in Table 3: the authors did not report any $r_f(G_{ox})$ [108,109]. However, as discussed in [109], for HTPB, Al addition at 5 wt.% has a small effect on r_f, while a 10 wt.% promoted a more sensible effect. For Sorbitol, Al load exhibited no marked influence on the fuel consumption rate. On the other hand, the relatively large data-scattering of SP1A prevents any consideration of the outcomes when loaded with 10 and 20 wt.% Al, under the investigated conditions. Similar considerations hold for the data discussed in [117]. This latter study considers N_2O and its mixtures with CO_2 for an HRE-based Mars Ascent Vehicle presenting non-metalized and metalized paraffin-based fuel data together with $r_f(G_{ox})$ of SP1A and SP7A formulations from Stanford. No details have been given on the selected paraffin, and the selected Al features a (nominal) particle size of 2 µm. Although the focus of the woork discussed in [117] is on the effects of CO_2 on the HRE combustion performance, the reference briefly analyze the behavior of the tested liquefying fuels in N_2O. No clear trend is noted when contrasting the non-metalized paraffin with the 40 wt.% Al-loaded counterpart over the G_{ox} range from 130 to 230 $kg/(m^2s)$.

In 2006, NASA, in collaboration with Stanford University and the Space Propulsion Group (SPG), launched a project to develop a 100 km nitrous oxide–paraffin hybrid rocket vehicle (named Peregrine) to carry a 5 kg payload to $>$ 100 km altitude [111]. The ground-test facility for Peregrine is detailed in [112], while Doran et al. [114] and Zilliac et al. [115] discuss details for the static firing tests of the engine. Efforts toward combustion efficiencies of around 95% are reported in these publications, with a limited discussion on the solid-fuel ballistics, but with relevant information on combustion instabilities.

In 2012, a rocket student team from Stanford University designed a medium-scale hybrid rocket using paraffin fuel and Nytrox (a mixture of oxygen and N_2O) [116]. Two ground firing tests were performed to evaluate the performance of the engine, with nitrous oxide replacing the original oxidizer. A discussion of Nytrox follows at the end of this Section.

European efforts for N_2O-based sounding rockets include the results from the HEROS (Hybrid Experimental Rocket Stuttgart) project [105], a project exploiting paraffin-based fuel that achieved three successful launches over four years of the project's duration, and the activities of the Delft Aerospace Rocket Engineering (DARE) of TU Delft [118–123]. In the most recent DARE activities, a N_2O-Sorbitol propellant combination has been developed.

Nitrous oxide was used by Lee and Tsai [124] to characterize the burning behavior of 50% paraffin wax + 50% HTPB mixture fuel (known as 50P). Under the investigated conditions, the performance of the hybrid rocket was reported to be similar to the gaseous oxygen case in terms of r_f values (providing the $r_f(G_{ox})$ shown in Table 3), though the use of N_2O as an oxidizer yielded lower specific impulse.

A 1 kN lab-scale HRE has been exploited by Grosse [72] to study the effect of diaphragms on combustion efficiency and the regression rate of the same. The tested diaphragms differ in geometry (featuring one and four perforations) and were placed at different locations along the fuel grain. Taking as baseline the performance of the grain without diaphragms, under the investigated conditions presented in [72], the r_f downstream of the diaphragm at the 33%-grain length position featured a 40% increase at 250 kg/(m^{2}s) for the one-hole diaphragm. Such a performance enhancement reached an 84% increase at 180 kg/(m^{2}s) for the four-hole diaphragm. Interestingly, positioning the four-hole diaphragm at 24% or 33% of the overall grain length produced the same combustion efficiency as the case where the insert is located at the grain end (before the aft-combustion chamber, which is the conventional location for such a device). In all these cases, the specific impulse of the system reached values close to 2021 m/s. The gain compared to the case without a diaphragm is estimated to be around 12% [72]. Enhanced propellant mixing and heat transfer justify the interesting and organically discussed results presented in [72]. This work was then extended by Bettella et al. [125], with a good agreement of the achieved results from the lab to intermediate scale.

The ballistic response of paraffin-based blends was investigated by Liu et al. [30] with both GOX and N_2O. In the study, a fuel blend (65P in Table 3) composed of paraffin (65 wt.%), PE (4 wt.%), HTPB (15 wt.%), Al (10 wt.%), Mg (5 wt.%), and $Cu_2Cr_2O_5$ (1 wt.%) was investigated for regression rate determination in a lab-scale engine with an injection swirl geometrical number of $SN_g = 6.83$. No details are given in the paper about the metal powder particle sizes. In this study, the $r_f(G_{ox})$ of Equation (1) yields a larger n_r value for GOX than N_2O. Such a result is justified by Liu et al. when considering the high oxidation capacity and the lower heat required during the injection of this oxidizer compared with the N_2O. Under the operating conditions tested in [30], the r_f of the 65P formulation exhibited no significant differences between the two oxidizers. The typical gasification surface profile observed with swirl injection, with a pit in the proximity of the oxidizer inlet [36,61–63], characterizes the post-firing grains of this study.

The effects of oxidizer-injection geometry on the performance of a 1 kN paraffin/N_2O HRE was investigated in [126]. Showerhead, hollow-cone, pressure-swirl, and vortex injectors were compared. The fastest r_f was achieved with a vortex injector. The results are due to the higher residence time promoted by the vortex flow, together with higher mass fluxes reached in operations with this injector configuration. The evaluation of different showerhead injection systems is reported by the same research group [127]. In this work, the same engine and propellant composition employed by the authors in [126] is considered. Showerhead injectors with injection holes were tested in the range 0.8 to 1.8 mm for several channels spanning from 71 to 11. The injector with the smallest orifice size showed the fastest regression rate and produced the $r_f(G_{ox})$ power-law approximation reported in Table 3. This injector also provided the highest efficiencies in terms of characteristic velocities, with values in the range 85% to 95%, with a G_{ox} dependence (the higher the mass flux, the higher the efficiency).

The same microcrystalline paraffin wax that was tested by Grosse [72] was used as fuel in a vortex flow HRE with 1 kN thrust presented by Bellomo et al. [128]. The work discusses experimental results studying the effects of tangential vortex oxidizer injection, evaluating different pre- and post-combustion-chamber configurations. Vortex injection effects are contrasted with the standard (axial) flow case. Vortex injector details given by the authors in [128] show a configuration with six inlets with a diameter of 1.2 mm, and an injector channel of 25 mm. The latter diameter coincides with the grain port diameter in the absence of a pre-combustion chamber. Vortex injection decreased pressure oscillations compared to

the axial case from 7% to 4%. At the same time, a 40% regression rate increase was achieved, for a reported a_r enhancement of 67% (n_r being arbitrarily set to 0.5 in this study, given the neutral trend of $p_c(t)$). Using diaphragms, the reported r_f enhancement was in the region of 6%. Combustion efficiency reached 96% when combining the vortex injection with a diaphragm at the end of the grain. The achieved results proved: (i) the impact of propellant mixing before expansion; and (ii) the stronger impact on r_f enhancement of vortex injection compared to the use of diaphragms.

Nardozzo et al. [129] used N_2O as an oxidizer to conduct counterflow diffusion flame experiments with HTPB fuel. These tests aimed to investigate the effect of pressure on the r_f of hybrid fuels. The fuel r_f was found to slightly increase for increasing chamber pressure. This result contrasts with what was achieved by the authors in [55], where HTPB showed $r_f \propto 1/p_c$. However, this different behavior could be due to the use of a different oxidizer (GOX) or the loading of metal in the fuel.

A comparison between the ballistic response of HTPB-based fuels burning in gaseous O_2 and N_2O was reported by Carmicino et al. [130]. In the same work, the r_f of metalized HTPB formulations are contrasted with those of paraffin-based fuels. Tests were performed in an HRE with a showerhead injector and grains with single-port perforation. Non-metalized HTPB showed no r_f dependence on the oxidizer tests. The addition of micron- and nano-sized Al to HTPB (with mass fractions of 3 and 12.8%) promoted regression rate and mass burning rate enhancements for tests in N_2O. As reported in the original paper, this result features good agreement with other relevant literature data on HDPE combustion with the same oxidizers [108,131]. Micron-sized Al is a spherical powder with a mean diameter in the range of 6.5 to 8 µm. The nanometric powder is produced by electrical explosion of wires and features a particle size of 100 nm. The average regression rate enhancement for micron-sized Al was 25% over the non-metalized HTPB for oxidizer mass flux of 100 kg/(m^{2}s). Under the conditions tested by the authors in [130], the performance of nano-sized Al exhibited similar results to the coarser Al counterpart. The paraffin-based fuel formulation tested by Carmicino et al. is a blend of macrocrystalline paraffin wax with 15 wt.% styrene polymer [35,36]. Paraffin-based formulation enabled an 80% regression rate increase over the metalized HTPB in the test conditions analyzed by the authors in [130]. As discussed by Carmicino et al., this result is possibly affected by the relatively low mechanical properties of the blend, causing solid-fuel sliver detachment.

Nytrox is a mixture of liquid N_2O and oxygen. The two gases are highly miscible in liquid phase. A detailed theoretical investigation of Nytrox is presented by the authors in [132].

Since vapor-phase N_2O can experience rapid thermal decomposition [133], Nytrox can be implemented to reduce such risk [95]. The maximization of the oxygen dilution in nitrous oxide requires a storage condition at 273 K of 0.9 MPa (higher than the corresponding N_2O vapor pressure). A discussion on the ignition and combustion of electrical arc-ignited 3D-printed ABS fuel grains burning with N_2O and gaseous oxygen is reported in [95,134,135]. In particular, in these latter works Nytrox 87 (87 wt.% N_2O, with 13 wt.% O_2) is used as an oxidizer in comparison with oxygen.

From data given by in [95], the Nytrox 87-ABS regression rate is moderately lower than for GOX/ABS (−25%). This result is primarily due to the reduced flame temperature and the associated heat transfer from the flame zone to the fuel surface. However, under the investigated conditions presented in [95], the r_f of Nytrox 87-ABS is nearly doubled compared to the N_2O case. Despite its acceptable performances, the Nytrox/ABS propellants exhibit mean ignition latencies that are significantly larger than for gaseous oxygen: 0.9 s versus 0.3 s [95]. However, in actual systems, these delays could have a limited impact when considering relatively long firing times. Multiple prototype ground-test units with thrust levels varying from 4.5 N to 900 N have been developed and tested by Whitmore et al. [95,134,135].

Table 3. Regression rate vs. oxidizer mass flux data of solid fuels with N_2O as an oxidizer [see Equation (1)]: $a_r = [\frac{mm}{s}/(\frac{kg}{m^2s})^{n_r}]$, with $G_{ox} = \left(\frac{kg}{m^2s}\right)$, except where otherwise stated.

Fuel	a_r	n_r	Ref.	Notes
SP-1a (Paraffin Wax)	0.155	0.50	[136]	
	0.178	0.50	[107]	
SP-7	0.078	0.545	[117]	
Sasol 0907 w/o diaphragm	0.132	0.56	[72]	Commercial paraffin wax (microcrystalline): congealing point 356–367 K, assumed as $C_{50}H_{102}$.
Sasol 0907 w 1-hole diaphragm, pre-grain	0.162	0.49	[72]	
Sasol 0907 w 1-hole diaphragm, post-grain	0.539	0.36	[72]	
Sasol 0907 w 4-hole diaphragm, pre	0.145	0.54	[72]	$75\ \frac{kg}{m^2s} < G_{ox} < 325\ \frac{kg}{m^2s}$
Sasol 0907 w 4-hole diaphragm, post	0.293	0.52	[72]	
Paraffin	0.159	0.784	[127]	$46\ \frac{kg}{m^2s} < G_{ox} < 51\ \frac{kg}{m^2s}$
50P	0.115	0.504	[124]	Fuel formulation with 50 wt.% Paraffin + 50 wt.% HTPB $125\ \frac{kg}{m^2s} < G_{ox} < 475\ \frac{kg}{m^2s}$
65P	0.088	0.395	[30]	Fuel formulation with 65 wt.% Paraffin + 15 wt.% HTPB + 4 wt.% PE + 5 wt.% Mg + 10 wt.% Al + 1 wt.% Copper Cromite $91\ \frac{kg}{m^2s} < G_{ox} < 242\ \frac{kg}{m^2s}$
Paraffin + SEBS-MA	0.072	0.77	[36,130]	Macrocrystalline wax, 15 wt.% SEBS-MA $30\ \frac{kg}{m^2s} < G_{ox} < 100\ \frac{kg}{m^2s}$
Sorbitol	0.286 [a]	0.310 [a]	[108]	$4\ \frac{g}{cm^2s} < G_{ox} < 15\ \frac{g}{cm^2s}$
HTPB	0.198 [a]	0.325 [a]	[108]	$5\ \frac{g}{cm^2s} < G_{ox} < 14\ \frac{g}{cm^2s}$
	0.417 [a]	0.347 [a]	[109]	$5\ \frac{g}{cm^2s} < G_{ox} < 23\ \frac{g}{cm^2s}$
	0.008	0.77	[95]	$5\ \frac{g}{cm^2s} < G_{ox} < 50\ \frac{g}{cm^2s}$
	0.020	1.09	[36]	Vortex flow pancake (VFP) HRE operating in fuel-rich conditions. $4.5\ \frac{g}{cm^2s} < G_{tot} < 7.5\ \frac{g}{cm^2s}$
HDPE	0.104 [a]	0.352 [a]	[108]	$2.5\ \frac{g}{cm^2s} < G_{ox} < 25\ \frac{g}{cm^2s}$
	0.248 [a]	0.331 [a]	[109]	$2.5\ \frac{g}{cm^2s} < G_{ox} < 27.5\ \frac{g}{cm^2s}$
	0.013	0.875	[137]	$77\ \frac{g}{cm^2s} < G_{ox} < 191\ \frac{g}{cm^2s}$
PMMA	0.111 [a]	0.377 [a]	[108]	$2.5\ \frac{g}{cm^2s} < G_{ox} < 27\ \frac{g}{cm^2s}$
	0.284 [a]	0.335 [a]	[109]	$2.5\ \frac{g}{cm^2s} < G_{ox} < 30\ \frac{g}{cm^2s}$
ABS	0.007 [b]	0.80 [b]	[95]	$5\ \frac{g}{cm^2s} < G_{ox} < 50\ \frac{g}{cm^2s}$

[a] $r_f = [\frac{mm}{s}]$, $G_{ox} = [\frac{g}{cm^2s}]$. [b] $r_f = [\frac{cm}{s}]$, $G_{ox} = [\frac{g}{cm^2s}]$.

3.2. Hydrogen Peroxide

Hydrogen peroxide is a green oxidizer, liquid at ambient temperature. In contrast to pure nitrous oxide, H_2O_2 is not used in its pure form, but is typically blended in a water solution to reduce hazards in case of accidents. Usually, H_2O_2 self-decomposes at a rate of $\sim$ 1%/year. Reduced rates are observed for high concentrations [94]. Currently, technologies allow the refinement of high-purity concentrations (99.99%), referred to as high-test peroxide (HTP). However, only concentrations up to 98% have been tested and implemented in sounding rockets. HTP has an active $O_2 > 125\%$ compared to N_2O, and its density is superior to LOX (Table 1). Specific impulse is slightly better than nitrous oxide, but H_2O_2 is characterized by a decomposition that leads to relatively low temperatures, with $1000 \lesssim T \lesssim 1200$ K (Table 1). A promising feature of hydrogen peroxide lies in the use of its catalytic decomposition to reach auto-ignition temperature inside the combustion chamber and to start combustion without requiring an igniter. Except for the last reference, all the authors reported in Table 4 adopt this system. An alternative solution to the use of an external device (igniter) and a catalytic bed has been proposed by Whitmore et al. [138], by exploiting electrostatic fields stored in ABS fuel layers.

Focusing on exhaust plume composition as observed by equilibrium thermochemistry reported in Figure 3, high concentrations of H_2O_2 result in lower CO and CO_2 levels than LOX and N_2O oxidizers. However, H_2O significant emission could cause an environmental impact in the form of instantaneous radiative force (see Section 2.4).

Due to the lower accessibility and more difficult management of hydrogen peroxide compared to nitrous oxide, its application is not widely used. Although the latter is adopted by most of the student rocket groups working with HREs (Skyward Experimental Rocketry, Aris Space, HyEnd, PoliWRocket, DARE, etc.), there are no records of using H_2O_2. Among space companies, Gilmour Space Technologies is working on a three-stage hybrid rocket based on hydrogen peroxide as an oxidizer (Eris rocket) [139]. The Łukasiewicz Research Network—Institute of Aviation in Warsaw has designed ILR-33 Amber, a multistage using HTP and HDPE [140]. NAMMO Space works with 87.5% H_2O_2 and HTPB with its Nucleus Sounding Rocket [141].

Hydrogen peroxide was and is widely investigated due to its attractive properties as an oxidizer in HREs. An intensive literature review of the use of HTP in hybrid rocket engines was performed by Okninski et al. [13,94]. Table 4 is a review of the collection made in [94], extended with further developments on the topic from the past two years.

In the past two years, new studies have been published. Granado et al. [142] designed an algorithm to simulate the operational life of a hybrid rocket engine at different conditions and configurations. Results were compared with experimental data obtained from their engine, HYCAT, which operates with 87.5% H_2O_2 and HDPE.

Glaser et al. [137] studied a cylindrical discrete divergent–convergent fuel-grain configuration to decrease the O/F shift and enhance fuel–oxidizer mixing. Tests were performed with N_2O as well as with H_2O_2 and HDPE (in two different facilities). Nitrous oxide global average regression rate fits the formula $r_f = 0.013\, G_{ox}^{0.875}$, and H_2O_2 was tested on the HYCAT engine (the same as the previous reference) obtaining $r_f = 0.0003\, G_{ox}^{1.32}$. The latter engine showed a local r_f increase higher in the backward-facing steps than in forward-facing steps, in contrast to the N_2O engine. This different behavior probably lies in the different fuel lengths of the motor. Hydrogen peroxide performance with this fuel configuration surpasses the results found in [142], where the same motor with an axial grain shape was used.

Researchers at the Beihang University carried out an intensive investigation of hydrogen peroxide with a 95% concentration. Meng et al. [143] have studied the effects of adding aluminum and aluminum hydride to HTPB when using 95% H_2O_2. Zhao et al. [144] have worked with 98% H_2O_2 and PE, exploring thrust throttling. This was achieved by combining a flow-oriented throttleable injector cooperating with a cavitating controllable venturi. This movable injector, designed to drastically reduce the pressure drop among all operating conditions, worked stably during cold flow tests and after ignition. Zhu et al. [145]

have proposed an efficient design optimization method, considering random and interval uncertainties to conduct uncertainty analysis and optimize the design of a hybrid rocket motor with mixed uncertainty. Verification of the method was performed by firing an eco-friendly, non-toxic, and high-performance combination of 98% H_2O_2 and HTPB. Meng et al.'s most recent publication [146] focuses on simulating combustion surface regression through a numerical model powered by a Butterworth filter. The validation was performed through a firing test based on 98% HTP and HTPB. Wei et al. [147] carried out a deep numerical investigation to study a three-dimensional regression rate of an HRE single-port wagon-wheel fuel grain. A great contribution to the analysis was given by the computed tomography and image processing of the burnt grain. Tests were performed with 98% H_2O_2 and HTPB.

Yun et al. [148] used 90% hydrogen peroxide along with HDPE to study the influence of port diameter and the length of solid fuel on the performances. Characterization was based on the ratio of nozzle throat area to fuel port area (J) for the port diameter, and the ratio of grain length to port diameter (l) to design the fuel length. When $0.3 < J < 1$, $200 < G_{ox} < 500\,\mathrm{kg/(m^2s)}$. An increase of J was associated with a decrease in the fuel port diameter and strongly influences the regression rate. Optimum performance corresponded to $0.4 < J < 0.6$. An increase in l corresponded to an increase in combustion efficiency η_{c^*}, and O/F decreased, with the best results achieved for $l = 20$.

Table 4. Regression rate vs. oxidizer mass flux data of solid fuels with H_2O_2 as oxidizer [see Equation (1)]: $a_r = [\frac{mm}{s}/(\frac{kg}{m^2s})^{n_r}]$, with $G_{ox} = \left(\frac{kg}{m^2s}\right)$, except where otherwise stated. Ignition is through the catalytic bed and engines are characterized by a radial architecture, except where differently specified.

H_2O_2 Conc.	Fuel	a_r	n_r	Ref.	Notes [a]
84%	Paraffin	0.0344	0.9593	[149]	$111\,\frac{kg}{m^2s} < G_{ox} < 162\,\frac{kg}{m^2s}$
85%	LDPE	0.0061	0.78	[150]	$70\,\frac{kg}{m^2s} < G_{ox} < 211\,\frac{kg}{m^2s}$, 0.69 *MPa*
		0.0294	0.52		$70\,\frac{kg}{m^2s} < G_{ox} < 211\,\frac{kg}{m^2s}$, 1.38 *MPa*
		0.0419	0.49		$141\,\frac{kg}{m^2s} < G_{ox} < 492\,\frac{kg}{m^2s}$, 2.76 *MPa*
87.5%	HDPE	0.0066	0.8159	[142]	$150\,\frac{kg}{m^2s} < G_{ox} < 400\,\frac{kg}{m^2s}$
87.5%	HDPE	0.0003	1.32	[137]	Axial with discrete divergent–convergent grain $150\,\frac{kg}{m^2s} < G_{ox} < 400\,\frac{kg}{m^2s}$
87.5%	PE	0.0446	0.3288	[151]	Vortex end-burning configuration
88%	PE	0.0072	0.8	[152]	$155\,\frac{kg}{m^2s} < G_{ox} < 400\,\frac{kg}{m^2s}$
90%	PE	-	0.45	[153]	Single-port, rod-and-tube, telescope geometry
90%	HTPB	0.0402	0.5623	[154]	$109\,\frac{kg}{m^2s} < G_{ox} < 255\,\frac{kg}{m^2s}$
90%	Paraffin blend	0.279 [a]	0.732 [a]	[155]	Fuel formulation with 50 wt.% Paraffin + 20 wt.% PE wax + 18 wt.% EVA + 10 wt.% SA + 2 wt.% Carbon
90%	HTPB + 60 wt.% Al	0.014 [b]	0.7 [b]	[156]	$116\,\frac{kg}{m^2s} < G_{ox} < 320\,\frac{kg}{m^2s}$
	HTPB + 60 wt.% Al-Mg	0.029 [b]	0.6 [b]		$148\,\frac{kg}{m^2s} < G_{ox} < 298\,\frac{kg}{m^2s}$

Table 4. *Cont.*

H_2O_2 Conc.	Fuel	a_r	n_r	Ref.	Notes [a]
90%	DCPD HTPB HTPB + 25 wt.% $NaBH_4$ HTPB + 50 wt.% $NaBH_4$ HTPB + 25 wt.% AlH_3	0.057 [b] 0.060 [b] 0.019 [b] 0.008 [b] 0.037 [b]	0.49 [b] 0.50 [b] 0.73 [b] 0.90 [b] 0.65 [b]	[157]	$281 \frac{kg}{m^2 s} < G_{tot} < 450 \frac{kg}{m^2 s}$
90%	Paraffin	0.145	0.5	[158]	
90% 95%	HDPE	0.0320 0.0074	0.54 0.75	[159]	$231 \frac{kg}{m^2 s} < G_{ox} < 409 \frac{kg}{m^2 s}$
90% 98%	HTPB	0.0939 0.0982	0.53 0.53	[160]	
98%	HTPB + 20 wt.% Al	0.0039	1.0433	[161]	Solid propellant igniter
	HTPB + 20 wt.% $C_{14}H_{10}$ + 20 wt.% Al	0.0043	1.0336		$75 \frac{kg}{m^2 s} < G_{ox} < 170 \frac{kg}{m^2 s}$
	HTPB + 28 wt.% Al + 10 wt.% Mg + 2 wt.% C	0.0267	0.7249		

[a] $r_f = [\frac{mm}{s}]$, $G_{ox} = [\frac{g}{cm^2 s}]$. [b] $r_f = a_r G_{tot}^{n_r}$.

4. Conclusions and Future Developments

A renewed interest in hybrid rocket propulsion has been fostered by current efforts toward green propellants. However, these systems feature a lower maturity level when compared to solid rocket motors and liquid rocket engines. The current work provides a review of the state of the art on currently ongoing test activities regarding HREs burning solid fuels with storable oxidizers such as N_2O and H_2O_2. In the analysis, special emphasis is given to paraffin-based fuels. The work aims to identify possible fields of research that may improve knowledge of hybrid rocket engine combustion from a greener perspective.

The work highlights some critical points surrounding the assessment of the environmental impact of HREs. First, there is a lack of detailed studies considering the impact of soot on engine emissions. Independently of the fuel considered, analysis of this aspect is relatively sparse. Similarly, improved knowledge is needed of the exhaust composition of HREs featuring metal loads. Despite the relatively low mass fraction typically considered in HREs, and in light of the relatively small mass fraction of CCPs expected in the exhaust, no open literature study provides an insight into the evolution and impact of particulates from a hybrid plume. Similarly, analyses on the exhaust plume–environment interaction is missing. These points should be addressed in further studies, to develop safer, cheaper, and greener propulsion systems.

Author Contributions: Conceptualization, C.P.; methodology, C.P. and A.H.; resources, A.H. and V.S.; data curation, A.H. and V.S.; writing—original draft preparation, C.P. and A.H.; writing—review and editing, C.P., V.S. and A.H.; visualization, A.H. and V.S. All authors have read and agreed to the published version of the manuscript.

Funding: This research received no external funding.

Conflicts of Interest: The authors declare no conflict of interest.

Abbreviations

The following abbreviations are used in this manuscript:

A-SOFT	Altering-intensity Swirling-Flow-Type
ABS	Acrylonitrile Butadiene Styrene
AMROC	American Rocket Company
AP	Ammonium Perchlorate
CCPs	Condensed Combustion Products
CFD	Computational Fluid Dynamics
CFP	Carbon Footprint
DARE	Delft Aerospace Rocket Engineering
GOX	Gaseous Oxygen
GWP	Global Warming Potential
HDPE	High-density Polyethylene
HEROS	Hybrid Experimental Rocket Stuttgart
HP	Hydrogen Peroxide
HRE	Hybrid Rocket Engine
HTP	High-Test Peroxide
HTPB	Hydroxyl-terminated Polybutadiene
iRF	Instantaneous Radiative Force
LH_2	Liquid Hydrogen
LOX	Liquid Oxygen
NA	Nitric Acid
NOx	Nitrogen Oxides
O/F	Oxidizer-to-fuel Ratio
PMMA	Polymethyl Methacrylate
RFNA	Red-fuming Nitric Acid
SPG	Space Propulsion Group
SPLab	Space Propulsion Laboratory
UV	Ultra Violet
VFP	Vortex Flow Pancake

References

1. Street, J.; Johnston, C.; Mansell, R.; Bloom, S. *Environmental Interactions of Hydrazine Fuels in Soil/Water Systems*; Final Report, March 1985–September 1987; Technical Report; Department of Soil Science, Florida University: Gainesville, FL, USA, 1988.
2. Hanning-Lee, M.A.; Brady, B.B.; Martin, L.R.; Syage, J.A. Ozone decomposition on alumina: Implications for solid rocket motor exhaust. *Geophys. Res. Lett.* **1996**, *23*, 1961–1964. [CrossRef]
3. Voigt, C.; Schumann, U.; Graf, K.; Gottschaldt, K.D. Impact of rocket exhaust plumes on atmospheric composition and climate—An overview. In *Progress in Propulsion Physics*; De Luca, L., Bonnel, K., Eds.; EDP Sciences: Les Ulis, France, 2013; Volume 4, Chapter 7, pp. 657–670. [CrossRef]
4. Dallas, J.; Raval, S.; Gaitan, J.A.; Saydam, S.; Dempster, A. The environmental impact of emissions from space launches: A comprehensive review. *J. Clean. Prod.* **2020**, *255*, 120209:1–120209:12. [CrossRef]
5. Ross, M.N.; Whitefield, P.D.; Hagen, D.E.; Hopkins, A.R. In situ measurement of the aerosol size distribution in stratospheric solid rocket motor exhaust plumes. *Geophys. Res. Lett.* **1999**, *26*, 819–822. [CrossRef]
6. Haeseler, D.; Bombelli, V.; Vuillermoz, P.; Lo, R.; Marée, T.; Caramelli, F. Green propellant propulsion concepts for space transportation and technology development needs. In Proceedings of the 2nd International Conference on Green Propellants for Space Propulsion (ESA SP-557), Cagliari, Italy, 7–8 June 2004.
7. Ross, M.; Toohey, D.; Peinemann, M.; Ross, P. Limits on the space launch market related to stratospheric ozone depletion. *Astropolitics* **2009**, *7*, 50–82. [CrossRef]
8. Chiaverini, M. Review of solid-fuel regression rate behavior in classical and nonclassical hybrid rocket motors. In *Fundamentals of Hybrid Rocket Combustion and Propulsion*, 1st ed.; Chiaverini, M., Kuo, K., Eds.; AIAA: Reston, VA, USA, 2007; Chapter 2, pp. 37–126. [CrossRef]
9. Karabeyoglu, M.; Altman, D.; Cantwell, B.J. Combustion of liquefying hybrid propellants: Part 1, general theory. *J. Propuls. Power* **2002**, *18*, 610–620. [CrossRef]
10. Karabeyoglu, M.; Cantwell, B.J. Combustion of liquefying hybrid propellants: Part 2, stability of liquid films. *J. Propuls. Power* **2002**, *18*, 621–630. [CrossRef]
11. Veale, K.; Adali, S.; Pitot, J.; Brooks, M. A review of the performance and structural considerations of paraffin wax hybrid rocket fuels with additives. *Acta Astronaut.* **2017**, *141*, 196–208. [CrossRef]

12. DeLuca, L.; Galfetti, L.; Maggi, F.; Colombo, G.; Merotto, L.; Boiocchi, M.; Paravan, C.; Reina, A.; Tadini, P.; Fanton, L. Characterization of HTPB-based solid fuel formulations: Performance, mechanical properties, and pollution. *Acta Astronaut.* **2013**, *92*, 150–162. [CrossRef]
13. Okninski, A.; Kopacz, W.; Kaniewski, D.; Sobczak, K. Hybrid rocket propulsion technology for space S revisited-propellant solutions and challenges. *FirePhysChem* **2021**, *1*, 260–271. [CrossRef]
14. Altman, D.; Holzman, A. Overview and history of hybrid rocket propulsion. In *Fundamentals of Hybrid Rocket Combustion and Propulsion*, 1st ed.; Chiaverini, M., Kuo, K., Eds.; AIAA: Reston, VA, USA, 2007; Chapter 1, pp. 1–36. [CrossRef]
15. Marquardt, T.; Majdalani, J. Review of classical diffusion-limited regression rate models in hybrid rockets. *Aerospace* **2019**, *6*, 75. [CrossRef]
16. Marxman, G.; Woolridge, C. Advances in tactical rocket propulsion. In Proceedings of the AGARD Colloquium on Progress in Tactical Rocket Propulsion, La Jolla, CA, USA, 22–23 April 1965.
17. Marxman, G.; Wooldridge, C.; Muzzy, R. Fundamentals of hybrid boundary-layer combustion. In *Heterogeneous Combustion*; Wolfhard, H., Glassman, I., Green, L., Eds.; AIAA: Reston, VA, USA, 1964; Volume 15, pp. 485–521. [CrossRef]
18. Marxman, G.; Gilbert, M. Turbulent boundary layer combustion in the hybrid rocket. *Symp. (Int.) Combust.* **1963**, *9*, 371–383. [CrossRef]
19. Strand, L.; Jones, M.; Ray, R.; Cohen, N. Characterization of hybrid rocket internal heat flux and HTPB fuel pyrolysis. In Proceedings of the 30th Joint Propulsion Conference and Exhibit, Indianapolis, IN, USA, 27–29 June 1994. [CrossRef]
20. Chiaverini, M.; Kuo, K.; Peretz, A.; Harting, G.; Chiaverini, M.; Kuo, K.; Peretz, A.; Harting, G. Heat flux and internal ballistic characterization of a hybrid rocket motor analog. In Proceedings of the 33rd Joint Propulsion Conference and Exhibit, Seattle, WA, USA, 6–9 July 1997. [CrossRef]
21. Estey, P.; Altman, D.; McFarlane, J. An evaluation of scaling effects for hybrid rocket motors. In Proceedings of the 27th Joint Propulsion Conference, Sacramento, CA, USA, 24–26 June 1991. [CrossRef]
22. Risha, G.; Evans, B.; Boyer, E.; Kuo, K. Metals, energetic additives, and special binders used in solid fuels for hybrid rockets. In *Fundamentals of Hybrid Rocket Combustion and Propulsion*, 1st ed.; Chiaverini, M., Kuo, K., Eds.; AIAA: Reston, VA, USA, 2007; Chapter 10, pp. 413–456. [CrossRef]
23. Paravan, C. Nano-sized and mechanically activated composites: Perspectives for enhanced mass burning rate in aluminized solid fuels for hybrid rocket propulsion. *Aerospace* **2019**, *6*, 127. [CrossRef]
24. Pal, Y.; Mahottamananda, S.N.; Palateerdham, S.K.; Subha, S.; Ingenito, A. Review on the regression rate-improvement techniques and mechanical performance of hybrid rocket fuels. *FirePhysChem* **2021**, *1*, 272–282. [CrossRef]
25. Péres de Araújo, E.; José Maschio, L.; Henrique Gouvêa, L.; Gustavo Ferroni Pereira, L.; Vieira, R. Thermal, Viscosimetric and Thermomechanical Combined Assessment of Mixture Modelled Composite Fuels for Hybrid Propulsion. *Propellants Explos. Pyrotech.* **2022**, *47*, e202100314. [CrossRef]
26. Frederick Jr, R.A.; Whitehead, J.J.; Knox, L.R.; Moser, M.D. Regression rates study of mixed hybrid propellants. *J. Propuls. Power* **2007**, *23*, 175–180. [CrossRef]
27. Whitmore, S.A.; Walker, S.D.; Merkley, D.P.; Sobbi, M. High regression rate hybrid rocket fuel grains with helical port structures. *J. Propuls. Power* **2015**, *31*, 1727–1738. [CrossRef]
28. Story, G. Large-scale hybrid motor testing. In *Fundamentals of Hybrid Rocket Combustion and Propulsion*, 1st ed.; Chiaverini, M., Kuo, K., Eds.; AIAA: Reston, VA, USA, 2007; Chapter 13, pp. 513–552. [CrossRef]
29. Jens, E.T.; Karp, A.C.; Miller, V.A.; Hubbard, G.S.; Cantwell, B.J. Experimental Visualization of Hybrid Combustion: Results at Elevated Pressures. *J. Propuls. Power* **2020**, *36*, 33–46. [CrossRef]
30. Liu, L.l.; He, X.; Wang, Y.; Chen, Z.b.; Guo, Q. Regression rate of paraffin-based fuels in hybrid rocket motor. *Aerosp. Sci. Technol.* **2020**, *107*, 106269. [CrossRef]
31. Carrick, P.; Larson, C. Lab scale test and evaluation of cryogenic solid hybrid rocket fuels. In Proceedings of the 31st Joint Propulsion Conference and Exhibit, San Diego, CA, USA, 10–12 July 1995. [CrossRef]
32. Petrarolo, A.; Kobald, M.; Schlechtriem, S. Visualization of Combustion Phenomena in Paraffin-Based Hybrid Rocket Fuels at Super-Critical Pressures. In Proceedings of the 2018 Joint Propulsion Conference, Cincinnati, OH, USA, 9 November 2018. [CrossRef]
33. Debus, C.; Ruettgers, A.; Petrarolo, A.; Kobald, M.; Siggel, M. High-performance data analytics of hybrid rocket fuel combustion data using different machine learning approaches. In Proceedings of the AIAA Scitech 2020 Forum, Orlando, FL, USA, 6–10 January 2020. [CrossRef]
34. Kobald, M.; Ciezki, H.K.; Schlechtriem, S.; Toson, E.; De Luca, L. Evaluation of paraffin-based fuels for hybrid rocket engines. In Proceedings of the 50th AIAA/ASME/SAE/ASEE Joint Propulsion Conference, Cleveland, OH, USA, 28–30 July 2014. [CrossRef]
35. Paravan, C.; Galfetti, L.; Maggi, F. A critical analysis of paraffin-based fuel formulations for hybrid rocket propulsion. In Proceedings of the 53rd AIAA/SAE/ASEE Joint Propulsion Conference, Atlanta, GA, USA, 10–12 July 2017. [CrossRef]
36. Paravan, C.; Galfetti, L.; Bisin, R.; Piscaglia, F. Combustion processes in hybrid rockets. *Int. J. Energ. Mater. Chem. Propuls.* **2019**, *18*, 255–286. [CrossRef]
37. Kobald, M.; Schmierer, C.; Ciezki, H.; Schlechtriem, S.; Toson, E.; De Luca, L. Viscosity and regression rate of liquefying hybrid rocket fuels. *J. Propuls. Power* **2017**, *33*, 1245–1251. [CrossRef]

38. Tang, Y.; Chen, S.; Zhang, W.; Shen, R.; DeLuca, L.T.; Ye, Y. Mechanical modifications of paraffin-based fuels and the effects on combustion performance. *Propellants Explos. Pyrotech.* **2017**, *42*, 1268–1277. [CrossRef]
39. Battista, F.; Cardillo, D.; Fragiacomo, M.; Di Martino, G.D.; Mungiguerra, S.; Savino, R. Design and testing of a paraffin-based 1000 N HRE breadboard. *Aerospace* **2019**, *6*, 89. [CrossRef]
40. Nakagawa, I.; Hikone, S. Study on the regression rate of paraffin-based hybrid rocket fuels. *J. Propuls. Power* **2011**, *27*, 1276–1279. [CrossRef]
41. Kim, S.; Moon, H.; Kim, J.; Cho, J. Evaluation of paraffin–polyethylene blends as novel solid fuel for hybrid rockets. *J. Propuls. Power* **2015**, *31*, 1750–1760. [CrossRef]
42. Kumar, R.; Ramakrishna, P.A. Studies on EVA-Based Wax Fuel for Launch Vehicle Applications. *Propellants Explos. Pyrotech.* **2016**, *41*, 295–303. [CrossRef]
43. Mengu, D.; Kumar, R. Development of EVA-SEBS based wax fuel for hybrid rocket applications. *Acta Astronaut.* **2018**, *152*, 325–334. [CrossRef]
44. Thomas, J.C.; Paravan, C.; Stahl, J.M.; Tykol, A.J.; Rodriguez, F.A.; Galfetti, L.; Petersen, E.L. Experimental evaluation of HTPB/paraffin fuel blends for hybrid rocket applications. *Combust. Flame* **2021**, *229*, 111386. [CrossRef]
45. Wang, Y.; Hu, S.q.; Liu, X.l.; Liu, L.l. Boundary layer combustion of HTPB/paraffin fuels for hybrid propulsion applications. *Aerosp. Sci. Technol.* **2022**, *129*, 107850:1–107850:8. [CrossRef]
46. Bisin, R.; Paravan, C.; Alberti, S.; Galfetti, L. A new strategy for the reinforcement of paraffin-based fuels based on cellular structures: the armored grain—mechanical characterization. *Acta Astronaut.* **2020**, *176*, 494–509. [CrossRef]
47. Bisin, R.; Paravan, C. A new strategy for the reinforcement of paraffin-based fuels based on cellular structures: The armored grain — Ballistic characterization. *Acta Astronaut.* **2023**, *206*, 284–298. [CrossRef]
48. Thomas, J.C.; Rodriguez, F.A.; Petersen, E.L. Metallic Additives for Solid-Fuel Propulsion Applications. *Combust. Sci. Technol.* **2023**, *195*, 1279–1298. [CrossRef]
49. Karabeyoğlu, A., Performance additives for hybrid rockets. In *Chemical Rocket Propulsion*; De Luca, L.T., Shimada, T., Sinditskii, V.P., Calabro, M., Eds.; Springer International Publishing: Berlin/Heidelberg, Germany, 2017; pp. 139–163. [CrossRef]
50. Maggi, F.; Gariani, G.; Galfetti, L.; DeLuca, L.T. Theoretical analysis of hydrides in solid and hybrid rocket propulsion. *Int. J. Hydrogen Energy* **2012**, *37*, 1760–1769. [CrossRef]
51. Paravan, C.; Verga, A.; Maggi, F.; Galfetti, L. Accelerated ageing of micron-and nano-sized aluminum powders: Metal content, composition and non-isothermal oxidation reactivity. *Acta Astronaut.* **2019**, *158*, 397–406. [CrossRef]
52. Hermsen, R. Aluminum oxide particle size for solid rocket motor performance prediction. *J. Spacecr. Rockets* **1981**, *18*, 483–490. [CrossRef]
53. Carlotti, S.; Maggi, F. Experimental techniques for characterization of particles in plumes of sub-scale solid rocket motors. *Acta Astronaut.* **2021**, *186*, 496–507. [CrossRef]
54. Marothiya, G.; Ramakrishna, P. Utilization of mechanically activated aluminum in hybrid rockets. *J. Propuls. Power* **2018**, *34*, 1206–1213. [CrossRef]
55. Connell Jr, T.L.; Yetter, R.A.; Risha, G.A.; Huba, Z.J.; Epshteyn, A.; Fisher, B.T. Enhancement of Solid Fuel Combustion in a Hybrid Rocket Motor Using Amorphous Ti–Al–B Nanopowder Additives. *J. Propuls. Power* **2019**, *35*, 662–665. [CrossRef]
56. Connell, T.L., Jr.; Risha, G.A.; Yetter, R.A.; Roberts, C.W.; Young, G. Boron and polytetrafluoroethylene as a fuel composition for hybrid rocket applications. *J. Propuls. Power* **2015**, *31*, 373–385. [CrossRef]
57. Pal, Y.; Kumar, V.R. Physical and Ballistic Characterization of Aluminum-Loaded Paraffin Hybrid Rocket Fuels. *Energy Fuels* **2017**, *31*, 10133–10143. [CrossRef]
58. Lee, C.; Na, Y.; Lee, G. The enhancement of regression rate of hybrid rocket fuel by helical grain configuration and swirl flow. In Proceedings of the 41st AIAA/ASME/SAE/ASEE Joint Propulsion Conference & Exhibit, Tucson, AZ, USA, 10–13 July 2005. [CrossRef]
59. Saburo, Y.; Noriko, S.; Kousuke, H. Controlling parameters for fuel regression rate of swirling-oxidizer-flow-type hybrid rocket engine. In Proceedings of the 48th AIAA/ASME/SAE/ASEE Joint Propulsion Conference & Exhibit, Atlanta, GA, USA, 30 July–1 August 2012. [CrossRef]
60. Franco, M.; Barato, F.; Paccagnella, E.; Santi, M.; Battiston, A.; Comazzetto, A.; Pavarin, D. Regression rate design tailoring through vortex injection in hybrid rocket motors. *J. Spacecr. Rockets* **2020**, *57*, 278–290. [CrossRef]
61. Paccagnella, E.; Barato, F.; Pavarin, D.; Karabeyoğlu, A. Scaling parameters of swirling oxidizer injection in hybrid rocket motors. *J. Propuls. Power* **2017**, *33*, 1378–1394. [CrossRef]
62. Kumar, C.P.; Kumar, A. Effect of swirl on the regression rate in hybrid rocket motors. *Aerosp. Sci. Technol.* **2013**, *29*, 92–99. [CrossRef]
63. Paravan, C.; Glowacki, J.; Carlotti, S.; Maggi, F.; Galfetti, L. Vortex combustion in a lab-scale hybrid rocket motor. In Proceedings of the 52nd AIAA/SAE/ASEE Joint Propulsion Conference, Salt Lake City, UT, USA, 25–27 July 2016. [CrossRef]
64. Sakote, R.; Yadav, N.; Karmakar, S.; Joshi, P.C.; Chatterjee, A.K. Regression Rate Studies of Paraffin Wax-HTPB Hybrid Fuels Using Swirl Injectors. *Propellants Explos. Pyrotech.* **2014**, *39*, 859–865. [CrossRef]
65. Haag, G.S. *Alternative Geometry Hybrid Rockets for Spacecraft Orbit Transfer*; University of Surrey: Guildford, UK, 2001; pp. 1–24.

66. Saito, D.; Saburo, Y.; Hirata, K.; Sakurai, T.; Shiraishi, N. Combustion characteristics of paraffin-fueled swirling oxidizer-flow-type hybrid rocket engines. In Proceedings of the 48th AIAA/ASME/SAE/ASEE Joint Propulsion Conference & Exhibit, Atlanta, GA, USA, 30 July–1 August 2012. [CrossRef]
67. Shinohara, K.; Nakagawa, I. Regression rate characteristics of paraffin-based fuel under swirled oxidizer flow. In Proceedings of the 48th AIAA/ASME/SAE/ASEE Joint Propulsion Conference & Exhibit, Atlanta, GA, USA, 30 July–1 August 2012. [CrossRef]
68. Quadros, F.D.; Lacava, P.T. Swirl injection of gaseous oxygen in a lab-scale paraffin hybrid rocket motor. *J. Propuls. Power* **2019**, *35*, 896–905. [CrossRef]
69. Ozawa, K.; Kitagawa, K.; Aso, S.; Shimada, T. Hybrid Rocket Firing Experiments at Various Axial–Tangential Oxidizer-Flow-Rate Ratios. *J. Propuls. Power* **2019**, *35*, 94–108. [CrossRef]
70. Messineo, J.; Shimada, T. Theoretical investigation on feedback control of hybrid rocket engines. *Aerospace* **2019**, *6*, 65. [CrossRef]
71. Ozawa, K.; Shimada, T. Performance of Mixture-Ratio-Controlled Hybrid Rockets for Nominal Fuel Regression. *J. Propuls. Power* **2020**, *36*, 400–414. [CrossRef]
72. Grosse, M. Effect of a diaphragm on performance and fuel regression of a laboratory scale hybrid rocket motor using nitrous oxide and paraffin. In Proceedings of the 45th AIAA/ASME/SAE/ASEE Joint Propulsion Conference & Exhibit, Denver, CO, USA, 2–5 August 2009. [CrossRef]
73. Whitmore, S.A.; Walker, S.D. Engineering model for hybrid fuel regression rate amplification using helical ports. *J. Propuls. Power* **2017**, *33*, 398–407. [CrossRef]
74. Nagata, H.; Ito, M.; Maeda, T.; Watanabe, M.; Uematsu, T.; Totani, T.; Kudo, I. Development of CAMUI Hybrid Rocket to Create a Market for Small Rocket Experiments. *Acta Astronaut.* **2006**, *59*, 253–258. [CrossRef]
75. Viscor, T.; Kamps, L.; Yonekura, K.; Isochi, H.; Nagata, H. Large-scale CAMUI type hybrid rocket motor scaling, modeling, and test results. *Aerospace* **2021**, *9*, 1. [CrossRef]
76. Karabeyoğlu, A.; Toson, E.; Evans, B. Effect of "O/F Shift" on Combustion Efficiency. In Proceedings of the 50th AIAA/ASME/SAE/ASEE Joint Propulsion Conference, Cleveland, OH, USA, 28–30 July 2014. [CrossRef]
77. Teipel, U.; Förter-Barth, U. Rheology of nano-scale aluminum suspensions. *Propellants Explos. Pyrotech.* **2001**, *26*, 268–272. [CrossRef]
78. Aphale, S.S.; Budzinski, K.; Surina III, G.; DesJardin, P.E. Influence of O_2/N_2 oxidizer blends on soot formation and radiative heat flux in PMMA-air 2D slab burner for understanding hybrid rocket combustion. *Comb. Flame* **2021**, *234*, 111628. [CrossRef]
79. Whitmore, S.A. Plume Contamination Measurements of an Additively Printed, Green-Propellant Hybrid Thruster. *J. Propuls. Power* **2022**, *38*, 671–685. [CrossRef]
80. Wilcox, L.; Shine, K.; Hoskins, B. Radiative forcing due to aviation water vapour emissions. *Atmos. Environ.* **2012**, *63*, 1–13. [CrossRef]
81. IPCC Report AR6. Available online: https://report.ipcc.ch/ar6/wg3/IPCC_AR6_WGIII_Full_Report.pdf (accessed on 20 February 2023).
82. Casalino, L.; Ferrero, A.; Masseni, F.; Pastrone, D. Emission-Driven Hybrid Rocket Engine Optimization for Small Launchers. *Aerospace* **2022**, *9*, 807. [CrossRef]
83. Ruijgrok, G.J.; Van Paassen, D. *Elements of Aircraft Pollution*; Delft University Press: Delft, The Netherlands, 2005; pp. 1–410.
84. Malkin, M.S. *Environmental Impact Statement for the Space Shuttle Program*; Final Statement, April 1978; Technical Report for National Aeronautics and Space Administration (NASA): Washington, DC, USA, 1978.
85. Potter, A.E. *Proceedings of the Space Shuttle Environmental Assessment Workshop on Stratospheric Effects*; Technical Memorandum, January 1977; Technical Report for National Aeronautics and Space Administration (NASA): Washington, DC, USA, 1977.
86. Potter, A.E. Environmental effects of the Space Shuttle. *J. Environ. Sci.* **1978**, *21*, 15–21.
87. Leone, D.; Turns, S. Active chlorine and nitric oxide formation from chemical rocket plume afterburning. In Proceedings of the 32nd Aerospace Sciences Meeting and Exhibit, Reno, NV, USA, 10–13 January 1994. [CrossRef]
88. Ross, M.N.; Sheaffer, P.M. Radiative forcing caused by rocket engine emissions. *Earth's Future* **2014**, *2*, 177–196. [CrossRef]
89. "HyImpulse" Website. Available online: https://www.hyimpulse.de/en/projects/3-project-hyplox75 (accessed on 6 October 2022).
90. "T4i—Technology for Propulsion and Innovation" Website. Available online: https://www.t4innovation.com/teide-hybrid-propellant/ (accessed on 6 October 2022).
91. Faenza, M.; Boiron, A.J.; Haemmerli, B.; Verberne, C.J. The nammo nucleus launch: Norwegian hybrid sounding rocket over 100km. In Proceedings of the AIAA Propulsion and Energy 2019 Forum, Indianapolis, IN, USA, 19–22 August 2019. [CrossRef]
92. Heister, S.; Wernimont, E., Hydrogen peroxide, hydroxyl ammonium nitrate, and other storable oxidizers. In *Fundamentals of Hybrid Rocket Combustion and Propulsion*, 1st ed.; Chiaverini, M., Kuo, K., Eds.; AIAA: Reston, VA, USA, 2007; Chapter 11, pp. 457–488. [CrossRef]
93. Nosseir, A.E.; Cervone, A.; Pasini, A. Review of state-of-the-art green monopropellants: For propulsion systems analysts and designers. *Aerospace* **2021**, *8*, 20. [CrossRef]
94. Okninski, A.; Surmacz, P.; Bartkowiak, B.; Mayer, T.; Sobczak, K.; Pakosz, M.; Kaniewski, D.; Matyszewski, J.; Rarata, G.; Wolanski, P. Development of green storable hybrid rocket propulsion technology using 98% hydrogen peroxide as oxidizer. *Aerospace* **2021**, *8*, 234. [CrossRef]
95. Whitmore, S.A. Nytrox as "drop-in" replacement for gaseous oxygen in SmallSat hybrid propulsion systems. *Aerospace* **2020**, *7*, 43. [CrossRef]
96. C.C.O.H. Safety—"Oxidizers". Available online: https://safety.fsu.edu/safety_manual/oxidizers.pdf (accessed on 6 October 2022).

97. Thermophysical Properties of Fluid Systems, NIST Chemistry WebBook. Available online: https://webbook.nist.gov/chemistry/fluid/ (accessed on 21 April 2023).
98. Kamps, L.; Sakurai, K.; Saito, Y.; Nagata, H. Comprehensive data reduction for N_2O/HDPE hybrid rocket motor performance evaluation. *Aerospace* **2019**, *6*, 45. [CrossRef]
99. U.S. Environmental Protection Agency. "Greenhouse Gas Overview". Available online: https://www.epa.gov/enviro/greenhouse-gas-overview (accessed on 6 October 2022).
100. Zakirov, V.; Sweeting, M.; Goeman, V.; Lawrence, T. Surrey research on nitrous oxide catalytic decomposition for space applications. In Proceedings of the 14th AIAA/USU Conference on Small Satellites, Logan, UT, USA, 21–24 August 2000.
101. Zakirov, V.; Sweeting, M.; Lawrence, T.; Sellers, J. Nitrous oxide as a rocket propellant. *Acta Astronaut.* **2001**, *48*, 353–362. [CrossRef]
102. Kaiyang, L.; Jie, F.; Wei, S.; Bing, S.; Guobiao, C. Design and experimental research of a sub-Newton N_2O monopropellant thruster with inner-heater. *Chinese J. Aeronaut.* **2022**, *35*, 309–318.
103. Wallbank, J.; Sermon, P.; Baker, A.; Courtney, L.; Sambrook, R. Nitrous oxide as a green monopropellant for small satellites. In Proceedings of the 2nd International Conference on Green Propellants for Space Propulsion (ESA SP-557), Cagliari, Italy, 7–8 June 2004.
104. Carlotti, S.; Maggi, F. Evaluating New Liquid Storable Bipropellants: Safety and Performance Assessments. *Aerospace* **2022**, *9*, 561. [CrossRef]
105. Kobald, M.; Fischer, U.; Tomilin, K.; Petrarolo, A.; Schmierer, C. Hybrid experimental rocket stuttgart: A low-cost technology demonstrator. *J. Spacecr. Rockets* **2018**, *55*, 484–500. [CrossRef]
106. Sportillo, A. N_2O Thermal Decomposition: Reaction Kinetics and Design of a Dedicated Experimental Setup. Master's Thesis, Politecnico di Milano, Milan, Italy, 3 October 2018.
107. VanPelt, D.; Skinner, M.; Buchanan, A.; Gulman, R.; Chan, H.; Hopkins, J.; Karabeyoglu, M.A. Overview of a 4-inch OD paraffin-based hybrid sounding rocket program. In Proceedings of the 40th AIAA/ASME/SAE/ASEE Joint Propulsion Conference and Exhibit, Fort Lauderdale, FL, USA, 11–14 July 2004. [CrossRef]
108. Lohner, K.; Dyer, J.; Doran, E.; Dunn, Z.; Zilliac, G. Fuel regression rate characterization using a laboratory scale nitrous oxide hybrid propulsion system. In Proceedings of the 42nd AIAA/ASME/SAE/ASEE Joint Propulsion Conference & Exhibit, Sacramento, CA, USA, 9–12 July 2006. [CrossRef]
109. Doran, E.; Dyer, J.; Lohner, K.; Dunn, Z.; Cantwell, B.; Zilliac, G. Nitrous oxide hybrid rocket motor fuel regression rate characterization. In Proceedings of the 43rd AIAA/ASME/SAE/ASEE Joint Propulsion Conference & Exhibit, Cincinnati, OH, USA, 8–11 July 2007. [CrossRef]
110. McCormick, A.; Hultgren, E.; Lichtman, M.; Smith, J.; Sneed, R.; Azimi, S. Design, Optimization, and Launch of a 3" Diameter N_2O/Aluminized Paraffin Rocket. In Proceedings of the 41st AIAA/ASME/SAE/ASEE Joint Propulsion Conference & Exhibit, Tucson, AZ, USA, 10–13 July 2005. [CrossRef]
111. Dyer, J.; Doran, E.; Dunn, Z.; Lohner, K.; Bayart, C.; Sadhwani, A.; Zilliac, G.; Cantwel, B.; Karabeyoglu, A. Design and development of a 100km nitrous oxide/paraffin hybrid rocket vehicle. In Proceedings of the 43rd AIAA/ASME/SAE/ASEE Joint Propulsion Conference & Exhibit, Cincinnati, OH, USA, 8–11 July 2007.
112. Dunn, Z.; Dyer, J.; Lohner, K.; Doran, E.; Bayart, C.; Sadhwani, A.; Zilliac, G.; Karabeyoglu, A.; Cantwell, B. Test facility development for the 15,000 lb thrust peregrine hybrid sounding rocket. In Proceedings of the 43rd AIAA/ASME/SAE/ASEE Joint Propulsion Conference & Exhibit, Cincinnati, OH, USA, 8–11 July 2007.
113. Dyer, J.; Doran, E.; Zilliac, G.; Lohner, K.; Cantwell, B.; Karabeyoglu, A.; Marzona, M.; Karlik, E. Status Update for the Peregrine 100km Sounding Rocket Project. In Proceedings of the 44th AIAA/ASME/SAE/ASEE Joint Propulsion Conference & Exhibit, Hartford, CT, USA, 21–23 July 2008.
114. Doran, E.; Dyer, J.; Marzona, M.; Karabayaglu, A.; Zilliac, G.; Mosher, R.; Cantwell, B. Status update report for the Peregrine sounding rocket project: Part III. In Proceedings of the 45th AIAA/ASME/SAE/ASEE Joint Propulsion Conference & Exhibit, Denver, CO, USA, 2–5 August 2009. [CrossRef]
115. Zilliac, G.; Waxman, B.; Doran, E.; Dyer, J.; Karabeyoglu, A.; Cantwell, B. Peregrine hybrid rocket motor ground test results. In Proceedings of the 48th AIAA/ASME/SAE/ASEE Joint Propulsion Conference & Exhibit, Atlanta, GA, USA, 30 July–1 August 2012. [CrossRef]
116. Simurda, L.; Stober, K.; Boiron, A.; Hornstein, K.; Jens, E.; Fletcher, A. Design and development of a thrust vector controlled Paraffin/Nytrox hybrid rocket. In Proceedings of the 48th AIAA/ASME/SAE/ASEE Joint Propulsion Conference & Exhibit, Atlanta, GA, USA, 30 July–1 August 2012.
117. Kara, O.; Karakaş, H. Hybrid rockets with mixed N_2O/CO_2 oxidizers for Mars Ascent Vehicles. *Acta Astronaut.* **2020**, *175*, 254–267. [CrossRef]
118. Fraters, A.; Zandbergen, B.; Weustink, A.; Eiche, M.; Gerth, I.; Hermsen, R.; Huijsman, V.; Knop, T.; Powell, S.; Wildvank, R. Development of a Hybrid Rocket Engine for the Stratos II Project. In Proceedings of the 62nd International Astronautical Congress (IAC), Cape Town, South Africa, 3–7 October 2011.
119. Knop, T.; Zandbergen, B.; Cervone, A.; Huijsman, R.; Powell, S.; Werner, R.; Ehlen, J.; Lindemann, F.; Wink, J.; Becker, C.; et al. Sorbitol-Based Hybrid Fuel Studies with Nitrous Oxide for the Stratos II Sounding Rocket. In Proceedings of the 49th AIAA/ASME/SAE/ASEE Joint Propulsion Conference, San Jose, CA, USA, 14–17 July 2013. [CrossRef]

120. Fraters, A.; Cervone, A. Combustion Instabilities and Spontaneous Engine Operation Shifting in a High Mass Flux N_2O-PMMA Hybrid Rocket Engine. In Proceedings of the AIAA 2014 Space Propulsion Conference and Exhibition, Cologne, Germany, 19–22 May 2014.
121. Wink, J.; Cervone, A.; Knop, T.; Huijsman, R.; Powell, S.; Samarawickrama, K.; Fraters, A.; Werner, R.; Becker, C. Test Campaign on a 10 kN class sorbitol-based hybrid rocket motor for the Stratos II Sounding Rocket. In Proceedings of the AIAA 2014 Space Propulsion Conference and Exhibition, Cologne, Germany, 19–22 May 2014.
122. Knop, T.; Wink, J.; Huijsman, R.; Werner, R.; Ehlen, J.; Powell, S.; Zandbergen, B.; Cervone, A. Failure mode investigation of a sorbitol-based hybrid rocket flight motor for the Stratos II sounding rocket. In Proceedings of the 51st AIAA/SAE/ASEE Joint Propulsion Conference, Orlando, FL, USA, 27–29 July 2015. [CrossRef]
123. Van den Berg, P.; Barreiro, F.; Klop, C.L.; Van Strydonck, D.; Koehler, S. Development of a 25kN Hybrid Rocket Engine for the Stratos III Sounding Rocket. In Proceedings of the 69th International Astronautical Congress (IAC), Bremen, Germany, 1–5 October 2018.
124. Lee, T.S.; Tsai, H.L. Fuel regression rate in a paraffin-HTPB nitrous oxide hybrid rocket. In Proceedings of the 7th Asia-Pacific Conference on Combustion (ASPACC), Taipei, Taiwan, 24–27 May 2009.
125. Bettella, A.; Lazzarin, M.; Bellomo, N.; Barato, F.; Pavarin, D.; Grosse, M. Testing and CFD simulation of diaphragm hybrid rocket motors. In Proceedings of the 47th AIAA/ASME/SAE/ASEE Joint Propulsion Conference & Exhibit, San Diego, CA, USA, 31 July–3 August 2011. [CrossRef]
126. Bouziane, M.; Bertoldi, A.; Milova, P.; Hendrick, P.; Lefebvre, M. Performance comparison of oxidizer injectors in a 1-kN paraffin-fueled hybrid rocket motor. *Aerosp. Sci. Technol.* **2019**, *89*, 392–406. [CrossRef]
127. Bouziane, M.; Bertoldi, A.M.; Hendrick, P.; Lefebvre, M. Experimental investigation of the axial oxidizer injectors geometry on a 1-kN paraffin-fueled hybrid rocket motor. *FirePhysChem* **2021**, *1*, 231–243. [CrossRef]
128. Bellomo, N.; Faenza, M.; Barato, F.; Bettella, A.; Pavarin, D.; Selmo, A. The "Vortex Reloaded" project: Experimental investigation on fully tangential vortex injection in N_2O-paraffin hybrid motors. In Proceedings of the 48th AIAA/ASME/SAE/ASEE Joint Propulsion Conference & Exhibit, Atlanta, GA, USA, 30 July–1 August 2012. [CrossRef]
129. Nardozzo, P.K.; Connell, T.L., Jr.; Boyer, E.; Yetter, R.; Young, G. Diffusion flame studies of solid fuels with nitrous oxide. *Int. J. Energetic Mater. Chem. Propuls.* **2020**, *19*, 73–93. [CrossRef]
130. Carmicino, C.; Scaramuzzino, F.; Sorge, A.R. Trade-off between paraffin-based and aluminium-loaded HTPB fuels to improve performance of hybrid rocket fed with N_2O. *Aerosp. Sci. Technol.* **2014**, *37*, 81–92. [CrossRef]
131. Carmicino, C. Acoustics, vortex shedding, and low-frequency dynamics interaction in an unstable hybrid rocket. *J. Propuls. Power* **2009**, *25*, 1322–1335. [CrossRef]
132. Karabeyoglu, M.A. Nitrous oxide and oxygen mixtures (nytrox) as oxidizers for rocket propulsion applications. *J. Propuls. Power* **2014**, *30*, 696–706. [CrossRef]
133. Rhodes, G. *Investigation of Decomposition Characteristics of Gaseous and Liquid Nitrous Oxide*; Final Report, August–December 1973. Technical Report for Air Force Weapons Laboratory: Kirtland Air Force Base, NM, USA, 1974.
134. Whitmore, S.A.; Frischkorn, C.I. Analyzing and Reducing Ignition Latency of a Nytrox/ABS Hybrid Propulsion System. In Proceedings of the AIAA Propulsion and Energy 2020 Forum, Virtual, 24–28 August 2020. [CrossRef]
135. Whitmore, S.A.; Stoddard, R.L. N_2O/O_2 blends safe and volumetrically efficient oxidizers for small spacecraft hybrid propulsion. *Aeron. Aero. Open Access J.* **2019**, *3*, 171–196. [CrossRef]
136. Karabeyoglu, A.; Zilliac, G.; Castellucci, P.; Urbanczyk, P.; Inalhan, G.; Cantwell, B. Flight Demonstration of the High Burning Rate Hydrocarbon-Based Hybrid Rocket Fuels. In Proceedings of the 39th AIAA/ASME/SAE/ASEE Joint Propulsion Conference and Exhibit, Huntsville, AL, USA, 20–23 July 2003. [CrossRef]
137. Glaser, C.; Gelain, R.; Bertoldi, A.; Levard, Q.; Hijlkema, J.; Lestrade, J.Y.; Hendrick, P.; Anthoine, J. Experimental regression rate profiles of stepped fuel grains in Hybrid Rocket Engines. *Acta Astronaut.* **2023**, *204*, 186–198. [CrossRef]
138. Whitmore, S.A.; Armstrong, I.W.; Heiner, M.C.; Martinez, C.J. High-performing hydrogen peroxide hybrid rocket with 3-D printed and extruded ABS fuel. In Proceedings of the 2018 Joint Propulsion Conference, Cincinnati, OH, USA, 9–11 July 2018. [CrossRef]
139. Gilmour Space Technologies. Eris Rocket. Available online: https://www.gspace.com/launch (accessed on 19 April 2023).
140. TriasRnD. ILR-33 AMBER 2K Rocket. Available online: https://triasrnd.com/1/358-ilr-33-amber-2k-rocket (accessed on 19 April 2023).
141. Nammo Space. Nucleus Sounding Rocket. Available online: https://www.nammo.com/product/nucleus-sounding-rocket/ (accessed on 19 April 2023).
142. Granado, E.Q.; Pelenghi, G.; Hijlkema, J.; Anthoine, J.; Lestrade, J.Y. A new System Design Tool for a Hybrid Rocket Engine Application. In Proceedings of the 73rd International Astronautical Congress (IAC), Paris, France, 18–22 September 2022.
143. Meng, X.; Tian, H.; Zhu, H.; Wang, Z.; Yu, R.; Guo, Z.; Cai, G. Effects of aluminum and aluminum hydride additives on the performance of hybrid rocket motors based on 95% hydrogen peroxide. *Aerosp. Sci. Technol.* **2022**, *130*, 107914:1–107914:9. [CrossRef]
144. Zhao, Z.; Cai, G.; Zhao, B.; Liu, Y.; Yu, N. Experimental investigation of a flow-oriented throttleable injector designed for throttleable hybrid rocket motor. *Acta Astronaut.* **2022**, *192*, 122–132. [CrossRef]
145. Zhu, H.; Xiao, M.; Zhang, J.; Cai, G. Uncertainty design and optimization of a hybrid rocket motor with mixed random-interval uncertainties. *Aerosp. Sci. Technol.* **2022**, *128*, 107791:1–107791:12. [CrossRef]

146. Meng, X.; Tian, H.; Chen, X.; Jiang, X.; Wang, P.; Wei, T.; Cai, G. Numerical simulation of combustion surface regression based on Butterworth filter in hybrid rocket motor. *Acta Astronaut.* **2023**, *202*, 400–410. [CrossRef]
147. Wei, T.; Cai, G.; Tian, H.; Jiang, X. Experiment and numerical research on regression rate of hybrid rocket motor with single-port wagon wheel fuel grain. *Acta Astronaut.* **2023**, *207*, 265–282. [CrossRef]
148. Yun, Y.; Kim, J.; Kwon, S. Parametric Study of Solid Fuel for Hydrogen Peroxide Hybrid Rocket Design. *J. Propuls. Power* **2022**, *38*, 229–240. [CrossRef]
149. Brown, T.R.; Lydon, M.C. Testing of Paraffin-Based Hybrid Rocket Fuel Using Hydrogen Peroxide Oxidizer. In Proceedings of the AIAA Region V Student Conference, Wichita, KS, USA, 15-16 January 2005 .
150. Wernimont, E.; Heister, S. Combustion experiments in hydrogen peroxide/polyethylene hybrid rocket with catalytic ignition. *J. Propuls. Power* **2000**, *16*, 318–326. [CrossRef]
151. Lestrade, J.Y.; Anthoine, J.; Musker, A.J.; Lecossais, A. Experimental demonstration of an end-burning swirling flow hybrid rocket engine. *Aerosp. Sci. Technol.* **2019**, *92*, 1–8. [CrossRef]
152. Wernimont, E.J.; Meyer, S.E. Hydrogen peroxide hybrid rocket engine performance investigation. In Proceedings of the 30th Joint Propulsion Conference and Exhibit, Indianapolis, IN, USA, 27–29 June 1994. [CrossRef]
153. Moore, G.E.; Berman, K. A solid-liquid rocket propellant system. *J. Jet Propuls.* **1956**, *26*, 965–968. [CrossRef]
154. Cai, G.; Zeng, P.; Li, X.; Tian, H.; Yu, N. Scale effect of fuel regression rate in hybrid rocket motor. *Aerosp. Sci. Technol.* **2013**, *24*, 141–146. [CrossRef]
155. Wu, Y.; Yu, X.; Lin, X.; Li, S.; Wei, X.; Zhu, C.; Wu, L. Experimental investigation of fuel composition and mix-enhancer effects on the performance of paraffin-based hybrid rocket motors. *Aerosp. Sci. Technol.* **2018**, *82*, 620–627. [CrossRef]
156. Farbar, E.; Louwers, J.; Kaya, T. Investigation of metallized and nonmetallized hydroxyl terminated polybutadiene/hydrogen peroxide hybrid rockets. *J. Propuls. Power* **2007**, *23*, 476–486. [CrossRef]
157. Shark, S.; Pourpoint, T.; Son, S.; Heister, S. Performance of dicyclopentadiene/H_2O_2-based hybrid rocket motors with metal hydride additives. *J. Propuls. Power* **2013**, *29*, 1122–1129. [CrossRef]
158. Paccagnella, E.; Santi, M.; Ruffin, A.; Barato, F.; Pavarin, D.; Misté, G.A.; Venturelli, G.; Bellomo, N. Testing of a long-burning-time paraffin-based hybrid rocket motor. *J. Propuls. Power* **2019**, *35*, 432–442. [CrossRef]
159. Kang, S.; Lee, D.; Lee, E.; Kwon, S. Design and performance evaluation of hybrid rocket using 95 wt.% H_2O_2. In Proceedings of the 52nd AIAA/SAE/ASEE Joint Propulsion Conference, Salt Lake City, UT, USA, 25–27 July 2016. [CrossRef]
160. Cai, G.; Zhu, H.; Rao, D.; Tian, H. Optimal design of hybrid rocket motor powered vehicle for suborbital flight. *Aerosp. Sci. Technol.* **2013**, *25*, 114–124. [CrossRef]
161. Li, X.; Tian, H.; Yu, N.; Cai, G. Experimental investigation of fuel regression rate in a HTPB based lab-scale hybrid rocket motor. *Acta Astronaut.* **2014**, *105*, 95–100. [CrossRef]